Crustal-scale structural architecture, shortening, and exhumation of an active, eroding orogenic wedge (Chugach/St. Elias Range, southern Alaska)

Andrew Meigs,[1] Sarah Johnston,[1,2] John Garver,[3] and James Spotila[4]

Received 31 May 2007; revised 16 November 2007; accepted 27 March 2008; published 16 July 2008.

[1] Active mountain building associated with the accretion of the Yakutat microplate (YT) in southern Alaska is characterized through the combination of a new balanced cross section and new low-temperature cooling ages. This analysis constrains the amount and timing of shortening, the spatial and temporal trends of exhumation, and the interplay between structural development and exhumation. A fold-and-thrust belt comprising three principal thrust sheets (the Hope Creek, Sullivan, and an offshore thrust sheet from north to south) characterizes the YT internal structure, which has absorbed a minimum of ~82 km shortening. Assuming shortening and foreland basin development occurred contemporaneously, the shortening rate across the YT is ~13–14 mm/a after 5.6 Ma. Detrital apatite fission track ages, from south to north, are unreset along the southern edge of the Sullivan thrust sheet at the coast, are reset and have ages younger than 6.3 Ma within the thrust belt, and have reset cooling ages of ~13 Ma in the North American upper plate. Only the zircon samples from the northern, internal YT are potentially reset. Exhumation rates within the thrust belt vary from 0.3 ± 0.1 mm/a to 4 ± 1.8 mm/a. Combining the thermochronometric and structural data indicate that wedge exhumation since ~6 Ma is 500 km^2 and that particle trajectories have larger horizontal than vertical components. Whereas exhumation and shortening have been focused on the windward side of the Chugach/St. Elias Range since ~6 Ma, the cooling ages do not uniquely distinguish between orographically versus tectonically controlled erosion.
Citation: Meigs, A., S. Johnston, J. Garver, and J. Spotila (2008), Crustal-scale structural architecture, shortening, and exhumation of an active, eroding orogenic wedge (Chugach/St. Elias Range, southern Alaska), *Tectonics*, *27*, TC4003, doi:10.1029/2007TC002168.

1. Introduction

[2] The suggestion that climate and erosion govern the flow of rock through convergent orogenic belts has focused recent studies on the linkages between deformation and surface processes [e.g., *Brozovic et al.*, 1997; *England and Molnar*, 1990; *Willett*, 1999; *Zeitler et al.*, 2001]. For example, coupled erosion-deformation models predict that material flows toward the more erosive, wet side of an orogenic belt (Figure 1) [e.g., *Beaumont et al.*, 1992; *Koons*, 1990; *Willett*, 1999; *Willett et al.*, 1993], an asymmetry that reflects the orographic effect on rainfall [e.g., *Barros and Lettenmeir*, 1994]. Using the model view of orogenic development, which builds on original critical wedge theory [e.g., *Dahlen*, 1990; *Davis et al.*, 1983], it is expected that orogenic cross-sectional shape, accretion, sliding along the base, internal deformation and erosion are linked. Changes in orogenic taper and width result from changes in erosion rates, mass influx, sedimentary prism taper, convergence rates, and bedrock erodibility [*Boyer*, 1995; *Davis et al.*, 1983; *DeCelles and Mitra*, 1995; *Whipple and Meade*, 2006; *Willett*, 1999]. Following the predictions of these models, a first step in assessing the degree to which climate and tectonics are coupled is to constrain how exhumation and shortening are distributed within an orogenic belt. Characterization of rock flow paths and exhumation thus requires constraint of the structural architecture, timing of deformation, and magnitude of exhumation at the scale of individual structures [*Batt and Brandon*, 2002; *Brewer and Burbank*, 2006; *Ehlers and Farley*, 2003; *Willett et al.*, 2003].

[3] In this paper, the Chugach/St. Elias orogen of southern Alaska is investigated from the perspective of the structural and stratigraphic architecture and exhumation. We present new thermochronometric constraints on exhumation over time, a new balanced cross section documenting the internal structure, and the first quantitative estimate of internal shortening and shortening rates. The principal goals are to: (1) determine the trends of exhumation spatially across the orogen and with time; (2) quantify the amount of internal shortening; and (3) understand the nature of accretion and deformation by comparing the amount of material added and removed during orogenesis. These observations link the exhumation, major structures, and structural development of the orogen and provide new

[1]Department of Geosciences, Oregon State University, Corvallis, Oregon, USA.
[2]Now at Department of Geosciences, Princeton University, Princeton, New Jersey, USA.
[3]Department of Geology, Union College, Schenectady, New York, USA.
[4]Department of Geology, Virginia Polytechnic Institute and State University, Blacksburg, Virginia, USA.

0278-7407/08/2007TC002168

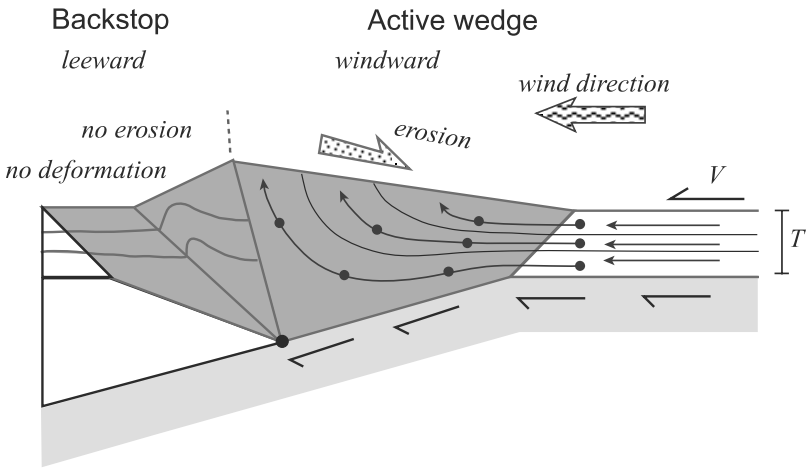

Figure 1. Coupled erosion deformation model of an end-member orogen type in which the tectonic influx of rocks into the orogen is from the same direction as moisture delivery, producing asymmetry in patterns of erosion and deformation (modified from *Willet et al.* [1993]). Rocks within the orogen are shaded dark gray, and undeformed rocks outside of the orogen are indicated by the stippled pattern. Light gray area at base represents subducted material that is not added to the orogen. Curved lines with arrows indicate particle trajectories, with dots representing equal time positions of particles. Note that the deepest level rocks are exhumed in the core on the windward side of the active wedge, that deeper rocks take longer to be exposed at the surface, and that material does not pass to the leeward flank of the wedge. T represents the thickness of incoming strata to be incorporated into the orogen, and V is convergence velocity.

insight into the relative importance of orography, erosion, and structure during active orogenic wedge development.

2. Chugach/St. Elias Orogen: Overview

2.1. Tectonic Setting

[4] The Chugach/St. Elias orogen (CSE) is located at a complex plate boundary and has attracted considerable interest because of the potential to study the interplay between climate, erosion, oblique convergence, and active terrane accretion [*Bruhn et al.*, 2004; *Meigs and Sauber*, 2000]. Along the active margin of southern Alaska, motion between the Pacific and North American plates switches from strike-slip along the Queen Charlotte/Fairweather fault system in the southeast to subduction along the Aleutian megathrust to the west (Figure 2) [*Plafker*, 1987]. Subduction/accretion of the Yakutat terrane (YT) into this margin is inferred to be the process most directly responsible for the growth of the St. Elias orogen [*Bruhn et al.*, 2004; *Lagoe et al.*, 1993; *Plafker*, 1987].

[5] The YT is a microplate that has moved north-northwest along the transform boundaries of southeast Alaska and British Columbia. Stratigraphic data suggest northward translation began after ~30 Ma associated with an eastward jump of the Pacific–North America transform plate boundary [*Plafker*, 1987]. Interpretations for the pretranslation location of the terrane range from relatively nearby in southeast Alaska/northern British Columbia [*Plafker et al.*, 1994b] to relatively far traveled having been displaced from as far south as California [*Bruns*, 1983]. Current motion of the YT from GPS data indicate the terrane is moving northwest with respect to North America [*Fletcher and Freymueller*, 1999; *Sauber et al.*, 1997]. Whereas the direction of motion of the YT and the Pacific plate relative to North America are similar [*DeMets et al.*, 1994; *Fletcher and Freymueller*, 1999; *Sauber et al.*, 1997], the YT is moving at a lower rate (~44 mm/a versus ~52 mm/a) and in a more westerly direction (Figure 2). Geophysical data indicate that the YT has subducted at least 500 km northwestward beneath the North American Plate in Alaska [*Eberhart-Phillips et al.*, 2006].

[6] Faults mark the contact between the YT, the North American upper plate, and the Pacific Plate (Figure 2) [*Bruhn et al.*, 2004; *Pavlis et al.*, 2004; *Plafker*, 1987; *Plafker et al.*, 1982]. In the east, the Fairweather Fault accommodates lateral motion between the YT and the Chugach terrane. On the north and west, the Prince William terrane is in fault contact with the YT (Figures 2–4). A thrust fault marks the northern contact (the Chugach/St. Elias thrust), whereas the western boundary is a complex zone marked by a normal fault onshore and the Kayak Island thrust fault zone offshore [*Bruhn et al.*, 2004]. The Chugach–St. Elias fault is an active thrust fault [*Estabrook et al.*, 1992], but the total displacement across it is unconstrained. The Pacific Plate–YT boundary is the Transition fault (Figure 2); the degree to which Pacific underthrusts YT is uncertain [*Bruns and Carlson*, 1987; *Eberhart-Phillips et al.*, 2006; *Gulick et al.*, 2007; *Pavlis et al.*, 2004; *Plafker et al.*, 1994a].

2.2. Orography and Topography

[7] Mean elevation of the CSE is ~1225 m, but increases along-strike from ~900 m at the Copper River in the west (~147.5°W) to >2500 m at ~140°W in the east (measured

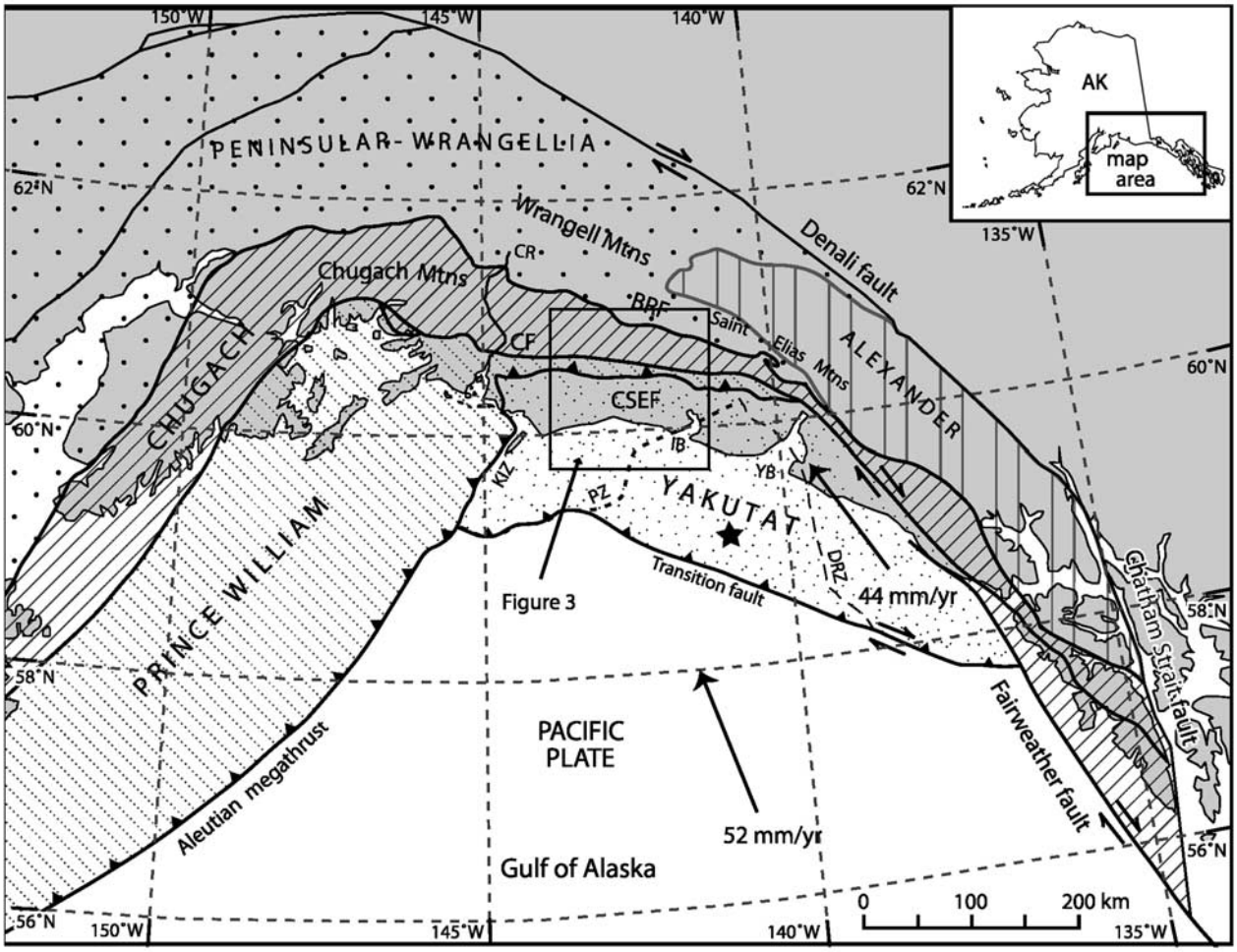

Figure 2. Regional map of southern Alaska showing major tectonic elements of the North American margin and Yakutat terrane [after *Plafker*, 1987; *Plafker et al.*, 1994a, 1994b]. Prince William, Chugach, Alexander, and Peninsular-Wrangellia are terranes accreted during the Paleozoic-Eocene. Present-day GPS velocities for the Pacific plate and Yakutat terrane are indicated [*Sauber et al.*, 1997; *Fletcher and Freymueller*, 1999; *DeMets et al.*, 1994]. CSEF, Chugach–St. Elias fault; CF, Contact fault; BRF, Border Ranges fault; KIZ, Kayak Island zone; PZ, Pamplona zone; DRZ, Dangerous River zone; YB, Yakutat Bay; IB, Icy Bay; and CR, Copper River. The Dangerous River zone may be an offset continuation of the Chatham Strait fault, which would constrain the northward displacement of the Yakutat terrane. A star on the continental shelf marks the location of well OCS-Y-211 [*Johnsson et al.*, 1992; *Plafker*, 1987]. Geology north of the Denali fault is not shown. Location of Figure 3 is indicated.

with distance east of the Copper River [*Meigs and Sauber*, 2000, Figure 9]). The highest relief and highest topography, including Mt. Logan (6050 m) and Mt. St. Elias (5490 m), coincide with the region of high mean elevation near 140°W. A combination of the high topography and close proximity to the Gulf of Alaska results in capture of a large percentage of the precipitation moving north off the Pacific Ocean (Figure 5) [*Mayo*, 1986; *Péwé*, 1975]. The abundant precipitation and high latitude explain the development of ice fields and tidewater glaciers (note the extent of glacial cover in Figure 3). Focused precipitation on the southern, windward flank of the CSE contributes to a low-elevation snow line on the south side of the range (Figure 5b) [*Mayo*, 1986]. Snow line serves as a proxy for the equilibrium line altitude (ELA) on glaciers; the location on the glacier where accumulation is equal to ablation and ice flux is greatest. Glacier sliding velocity is thought to scale with ice flux [*Andrews*, 1972; *Humphrey and Raymond*, 1994], which implies that glacial erosion rates peak within the elevation range of the ELA.

2.3. Exhumation

[8] Previous studies in the CSE have quantified erosion and exhumation on three spatial and temporal scales. Short-

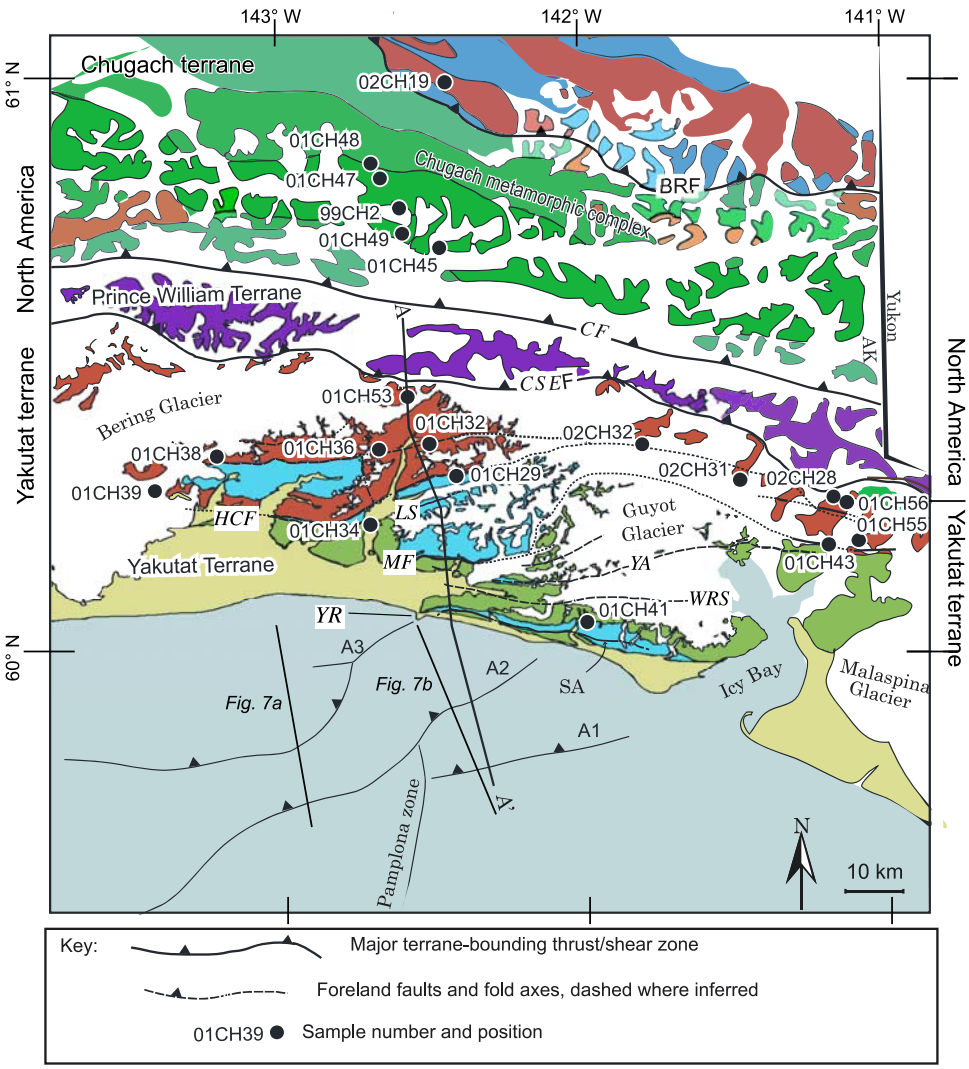

Figure 3. Geologic map of study area showing locations of all thermochronology samples (Figures 8 and 9 and Tables 1–3) and cross-section line A-A', shown in Figure 6. See Figure 4 for key to all stratigraphic units. The Chugach–St. Elias fault (CSEF) coincides with the orographic divide of the range (Figure 4). Seismic lines 409 and 406 of Figures 7a and 7b, respectively, are shown. Offshore faults are labeled with the names of associated anticlines given by *Bruns and Schwab* [1983]. Folds include the Sullivan anticline (SA, cut by the Sullivan fault on the south limb), the Yakataga anticline (YA), the Leeper syncline (LS), and the White River syncline (WRS). Major faults include the Miller Creek (MF) and Hope Creek (HCF) faults. Figure is after *Miller* [1971], *Plafker* [1987], and *Hudson and Plafker* [1982]. The orographic divide separating the windward and leeward flanks of the range coincides with the region of high peaks and high mean elevation between the Chugach/St. Elias and Contact faults [*Mayo*, 1986; *Meigs and Sauber*, 2000; *Péwé*, 1975].

term (10^1–10^2 year timescales) primary glacial erosion rates of 10 mm/a to 50 mm/a are inferred from tidewater glacier sediment yields and from the volume of sediment in sinks such as fjords [*Hallet et al.*, 1996]. Short-term records likely record short-lived, large-volume sediment pulses associated with landscape and glacier disequilibrium during Late Holocene climate change [*Koppes and Hallet*, 2002; *Meigs et al.*, 2006; *Meigs and Sauber*, 2000]. Intermediate timescale (10^4 year timescale) erosion rates estimated from the thickness of Holocene sediments on the Gulf of Alaska Continental Shelf suggest a regionally averaged sediment yield that is equivalent to a 2 to 5 mm/a erosion rate [*Sheaf et al.*, 2003]. Thus the intermediate timescale rate is roughly half the short-term rate.

[9] Long-term (10^6–10^7 year timescales) exhumation rates constrained by thermochronologic data are substantially lower than estimates on shorter timescales [*Berger and Spotila*, 2006; *O'Sullivan and Currie*, 1996; *Spotila et*

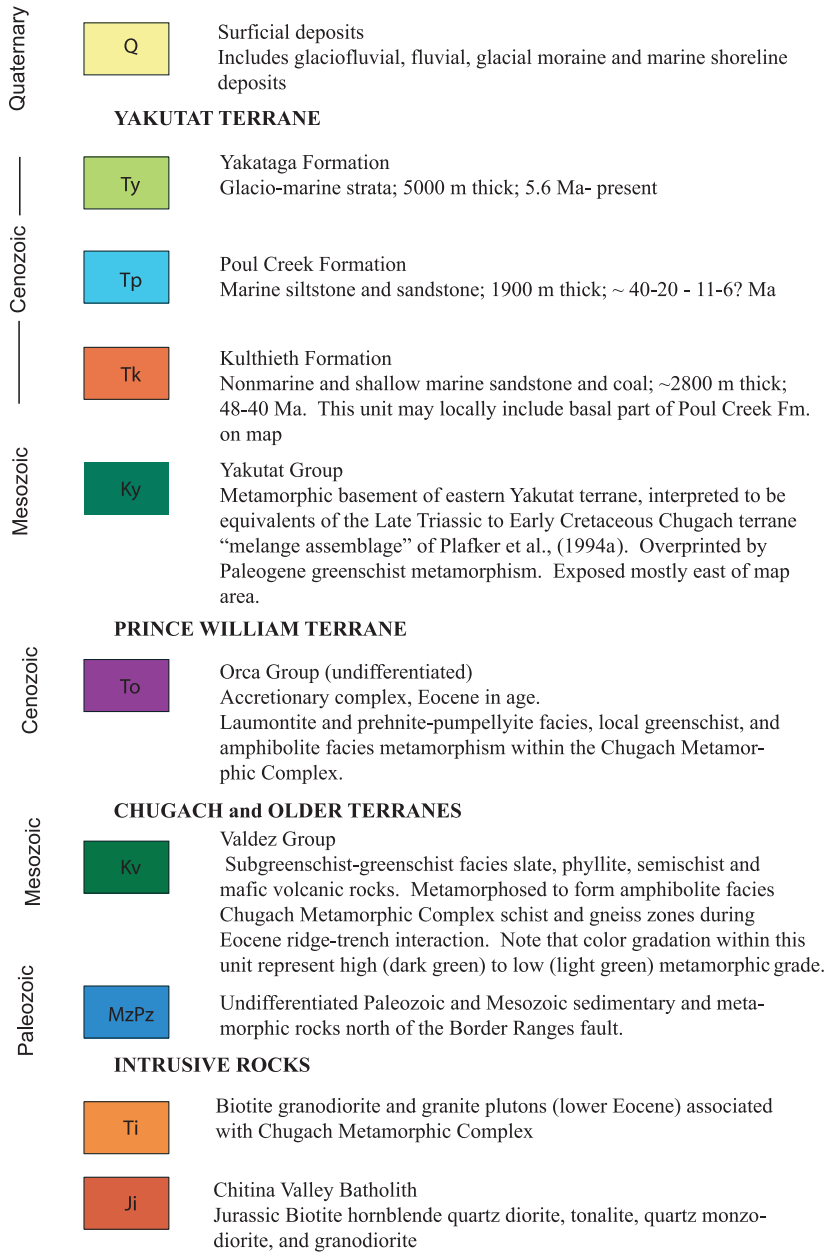

Figure 4. Map units for Figure 3. See text for descriptions of cover sedimentary units within the Yakutat terrane.

al., 2004]. Apatite fission track data from a vertical transect on Mt. Logan implies exhumation rates vary from 0.3 to 0.7 mm/a [*O'Sullivan and Currie*, 1996]. *Spotila et al.* [2004] and *Berger and Spotila* [2006] characterized the spatial pattern of exhumation throughout the orogen via a suite of apatite and zircon (U-Th)/He data and the existing apatite fission track data. Apatite (U-Th)/He data suggest average rates of 0.4–1.2 mm/a across the CSE, with local maxima up to ~4 mm/a. Exhumation is greatest within the actively deforming Yakutat fold-and-thrust belt to the south of the orographic divide (which coincides approximately with the Chugach–St. Elias fault; Figure 3). North of the orographic divide, total exhumation rates are substantially lower.

3. Yakutat Terrane Basement and Cover Rocks

[10] Thick sequences of marine and continental strata (~9500–10,000 m thick, Figure 4) overlie a complex basement assemblage in the YT [*Plafker*, 1987]. This study focuses on the YT west of the Dangerous River zone (DRZ) (Figures 2 and 3), a roughly north-south trending zone separates different types of basement: Accretionary com-

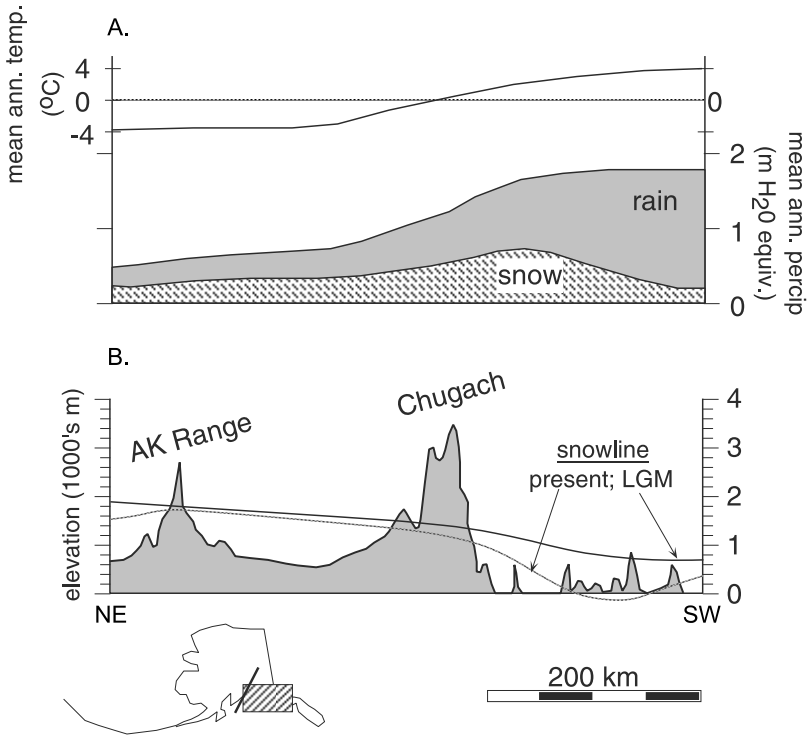

Figure 5. Orographic effect in the Chugach/St. Elias Range. (a) Mean annual precipitation and annual temperature plotted with distance. (b) Present and last glacial maximum snow lines plotted with topography. Snow line is the line on a glacier surface marking >50% surface cover by snow in the late summer and is used as a proxy for ELA (see text). Note the dramatic reduction in precipitation north of, and the low snow line south of, the Chugach Mountains. Figure is after *Péwé* [1975].

plex rocks inferred to be a fragment of the Chugach terrane form the YT basement west of the DRZ [*Plafker et al.*, 1994b]. Three units comprise the cover sequence of the YT [*Plafker*, 1987]. From oldest to youngest, these units are the Kulthieth, Poul Creek, and Yakataga Formations, respectively (Figure 4). Onshore these units have little or no evidence of metamorphism. Review of the thickness, age, and provenance of the cover sequence is relevant to both the balanced cross-section construction and to interpretation of the detrital thermochronometric ages.

3.1. Yakutat Terrane Cover Stratigraphic Succession: Kulthieth Formation

[11] The Kulthieth Formation (Tk) is dominated by sandstone, which is partly arkosic, includes coal interbeds, and has an uncertain thickness and age [*Miller*, 1971; *Plafker*, 1987]. Onshore, the unit records a marine regression, with nonmarine alluvial, delta plain, and shallow marine facies. Deeper marine facies characterize equivalent units offshore [*Plafker*, 1987]. Unit thickness is hard to determine and highly variable because no intact, little-deformed sections are exposed. Estimates from the type locality in the Yakataga area are 2800 m or greater [*Miller*, 1957; *Plafker*, 1987; *Wahrhaftig et al.*, 1994]. This thickness is consistent with the combined thicknesses of the better-known Poul Creek and Yakataga Formations and the ~10 km depth to basement in the undeformed foreland offshore [*Plafker*, 1987]. The depositional age of the Kulthieth Formation is not well constrained. Marine mollusk faunal and leaf floral data from the Kulthieth Formations and age-equivalent units in the Yakataga area suggest an age of Early Eocene to Early Oligocene (~55–28.5 Ma; [*Palmer and Geissman*, 1999]) [*Plafker*, 1987, p. 244, Figure 4].

3.2. Poul Creek Formation

[12] Strata of the Poul Creek Formation conformably overly the Kulthieth Formation. Low sediment accumulation rates represented by marine siltstones and sandstones intercalated with water laid tuffs, breccia and pillow lava. Poul Creek Formation deposition is interpreted to record a marine transgression [*Miller*, 1971; *Plafker*, 1987]. The unit is 1860 m thick in the Yakataga area [*Lagoe*, 1983; *Plafker*, 1987]. The age of the Poul Creek is late Eocene–early Miocene (~40–20 Ma) according to *Plafker* [1987]. *Lagoe et al.* [1993] revised the age of the top of the Poul Creek on the basis of a 5.6 Ma K/Ar date on an uppermost glauconite bed.

[13] Sandstone compositions of both the Kulthieth and Poul Creek Formations suggest a complex volcanic-arc provenance that includes plutonic and metamorphic sources [*Plafker et al.*, 1994b]. Given that the YT originated to the south of its present position [*Bruns*, 1983; *Plafker et al.*, 1994b], the most likely source of the preorogenic strata is the Coast Mountains of Alaska and British Columbia,

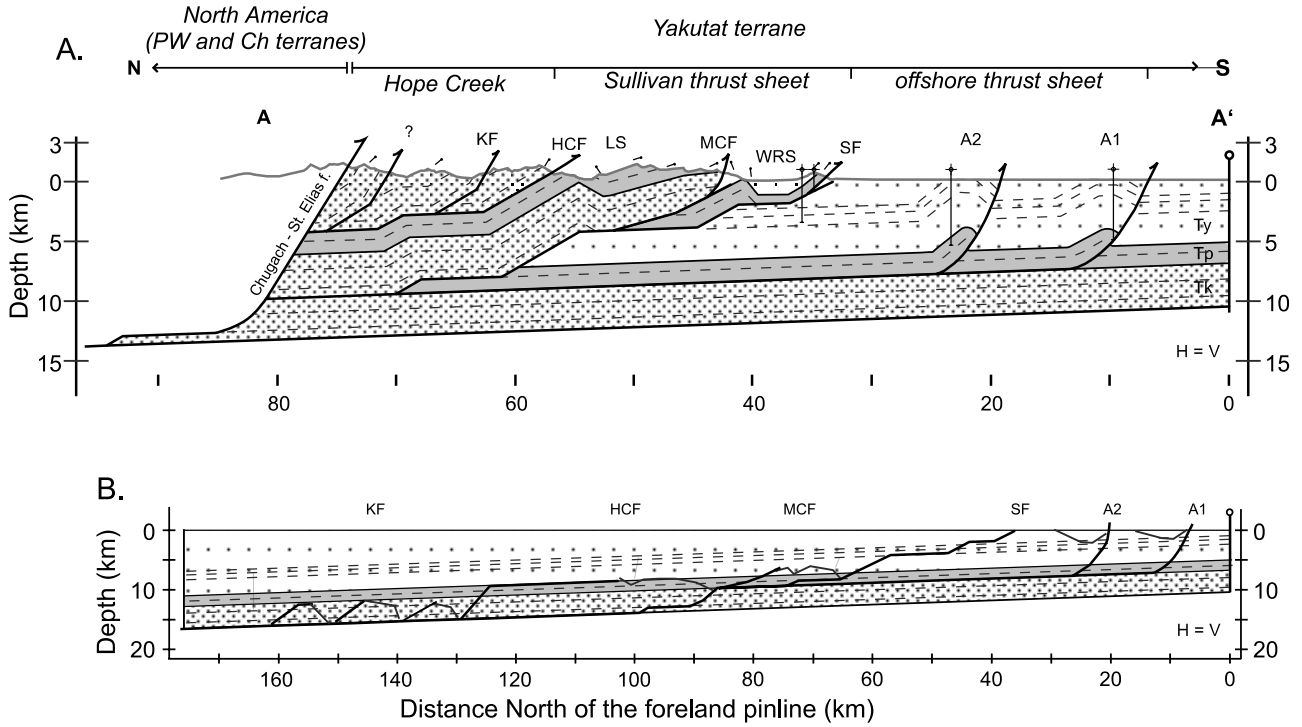

Figure 6. (a) Deformed state cross section through Yakutat fold-and-thrust belt. SF, Sullivan fault; WRS, White River syncline; MCF, Miller Creek Fault; LS, Leeper syncline; HCF, Hope Creek fault; KF, Kosakuts fault; Ty, Yakataga Fm.; Tp, Poul Creek Fm.; Tk, Kulthieth Fm. Anticlines A1 and A2 are the names used by *Bruns and Schwab* [1983] and are taken from seismic line 406 (Figure 7). Anticline A1 represents the active thrust front. Growth strata in the Yakataga Formation imaged on these anticlines are not depicted. (b) Restored state section, shown at 50% of original scale. Note that undeformed sedimentary taper is controlled by the 2° regional dip of the Yakataga Formation. Subsurface data constrain the structure of the offshore thrust sheet to ~5 km depth. Structural and stratigraphic data constrain the onshore thrust sheets to ~3 km depth. See text for data sources and assumptions.

including the nearby Chugach terrane. If the terrane traveled from a position farther south, it is likely that sediments would largely be drawn from the length of the British Columbia coast.

3.3. Yakataga Formation

[14] A thick package of synorogenic, glacial marine strata (the Yakataga Formation) overlie the Poul Creek Formation. Yakataga Formation sediments were deposited in the foreland basin formed contemporaneously with accretion and internal shortening of the YT [*Plafker*, 1987]. Seismic reflection lines and wells across the Yakataga Formation offshore indicate that its thickness ranges from 4000 to 6000 m; the thickness in the study area is ~5000 m [*Bruns and Schwab*, 1983]. Onshore at Yakataga Reef (Figure 3), the contact between Poul Creek and Yakataga is conformable, marked by a paucity of glauconitic beds, and an influx of coarser strata [*Lagoe*, 1983]. Elsewhere in the Robinson Mountains area, a slight angular unconformity marks the contact [*Miller*, 1971]. In contrast, offshore well data indicate the contact is an unconformity that separates mid-Pliocene glacial marine strata from deep water rocks of the Oligocene Poul Creek Formation [*Zellers*, 1993]. Magnetostratigraphic data, biostratigraphic data, and a 5.6 Ma age for the top of the Poul Creek Formation indicate the Yakataga Formation ranges in age from ~5.6 Ma to the present [*Lagoe et al.*, 1993; *Zellers*, 1993, 1995]. Provenance of the Yakataga Formation includes all potential sources in the CSE, including the Chugach and Prince William terranes in the North American upper plate and the Kulthieth and Poul Creek Formations (Figure 2). Glacial-marine deposits of the Yakataga Formation provide evidence for nearly continuous glaciation of the Chugach/St. Elias Range since 5.6 Ma [*Eyles et al.*, 1991; *Lagoe et al.*, 1993].

4. Internal Structure of the Yakutat Terrane

[15] A fold-and-thrust belt developed within the YT as the result of the ongoing collision with North America [*Miller*, 1971; *Plafker*, 1987]. *Bruhn et al.* [2004] divided the internal structures into three structural domains on the basis of along-strike variations in structural style and deformation history. Our study area and crustal-scale tran-

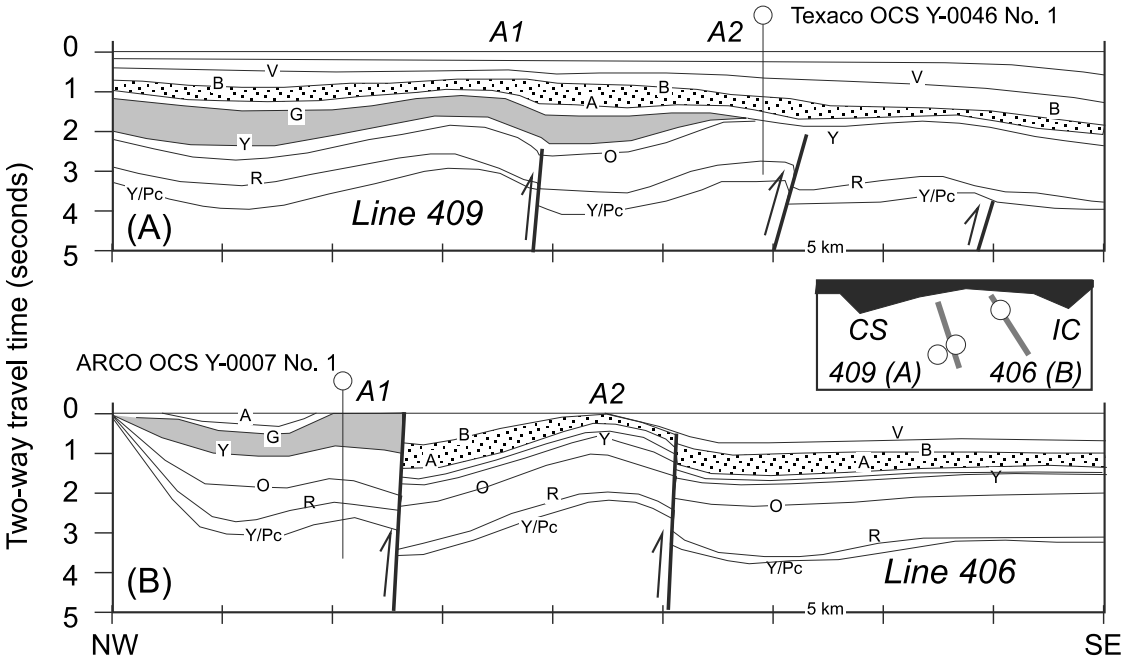

Figure 7. Line drawings of two seismic reflection profiles from the Gulf of Alaska depicting the leading edge of the thrust belt, stratal geometries, and ages of key horizons (modified from *Zellers* [1995]). From oldest to youngest, the age of the base of key horizons are: Y/PC (Yakutat–Poul Creek Formation contact) 5.35 Ma; O, ~2.5 Ma; Y, ~1.85 Ma (gray), ~0.78 Ma < A < 0.25 Ma; B, 0.25 Ma (stipple). Index map at upper right shows the positions of lines (a) 409 and (b) 406 from west to east, relative to Cape Suckling (CS) and Icy Cape (IC). The horizontal scale is in kilometers, and the vertical scale is in two-way travel time in seconds.

sect (Figures 3 and 6) are located within the "Central Segment," a zone where the sense of motion along major foreland faults and the Chugach–St. Elias fault is characterized by dip-slip motion. The Central Segment extends from Icy Bay on the east to the Bering Glacier on the west (Figure 3). A thin-skinned fold-and-thrust belt that involves the Cenozoic strata of the YT characterizes structure within the Central Segment. This fold-and-thrust belt extends from the Chugach–St. Elias thrust fault on the north to an active thrust front offshore on the south (the Pamplona zone/Malaspina thrust). The thrust front occurs within the YT. Growth strata indicate that deformation occurred throughout Yakataga Formation accumulation and that structures become progressively younger to the south offshore (Figure 7) [*Bruns and Schwab*, 1983; *Miller*, 1971; *Zellers*, 1993].

4.1. Cross-Section Location, Data Sources, and Assumptions

[16] Whereas the minimum duration of shortening and convergence of the YT with respect to North America are well constrained [*Bruns and Schwab*, 1983; *Eberhart-Phillips et al.*, 2006; *Lagoe et al.*, 1993; *Miller*, 1971; *Plafker*, 1987; *Plafker and Miller*, 1958; *Zellers*, 1993], the amount of internal deformation within the fold-and-thrust belt has not been quantified. To quantify internal shortening, a NNW-SSE oriented crustal-scale balanced cross section was drawn from the Chugach–St. Elias fault to the undeformed foreland offshore (Figure 6). This section is drawn entirely within the Yakutat terrane. We did not attempt to incorporate shortening and thickening present in the North American upper plate.

[17] Collision of the Yakutat terrane with North America is inherently a 3-D phenomenon [*Pavlis et al.*, 2004]. Both the cross-section location and orientation were explicitly chosen such that the sense of motion on major structures is along the line of section and out-of-plane motion is minimized. Our section crosses the dip slip dominated Central Segment of *Bruhn et al.* [2004], an area which includes the hypocenters of the principal events of the 1979 St. Elias earthquake sequence (the North America–Yakutat boundary) [*Estabrook et al.*, 1992]. The majority of the events have nearly pure dip-slip focal mechanisms. Our section orientation across the YT is nearly parallel to Yakutat–North America relative motion as indicated by GPS data (Figures 2 and 3) [*Fletcher and Freymueller*, 1999; *Sauber et al.*, 1997]. Thus, we assume that out-of-plane motion is not significant and that the cross section captures a significant fraction of the relative motion of Yakutat with respect to North America at the location of the section across the collision zone.

[18] Map data were compiled from *Miller* [1971], and constitutes the primary onshore data source used in the construction of the cross section. Seismic surveys conducted by the USGS in the offshore areas immediately adjacent and to the south of the Yakataga District [*Bruns and Schwab*, 1983] and later interpreted by *Zellers* [1993, 1995] were

used to constrain the offshore section of the transect (Figure 7). In particular, Line 406, which parallels our cross section, was used to interpret the structure from the coast across the thrust belt offshore (Figure 3). Well data from onshore wells, the White River 1 (Richfield Oil Corp.) and White River 2 and 3 (BP Exploration Co., Inc.) wells and two offshore wells, OCS Y-0007 (Arco) and OCS Y-0032 (Texaco) were also used [*Plafker*, 1987].

[19] Thickness of the stratigraphic section and the dip of the basement are key controls of the cross section. Thickness of the cover stratigraphic sequence is constrained by well and outcrop data for the Yakataga (5000 m) and Poul Creek Formations (1860 m), but not for the Kulthieth Formation (Figure 4). A ~2800 m thickness is assumed for the Kulthieth Formation as described in section 2.1. A 2° dip for the base of the cover stratigraphic sequence is indicated by field, seismic, and well data [*Plafker*, 1987]. Isopachs of the base of the Yakataga Formation indicate that the unit increases in thickness from the distal foreland offshore to the south to the proximal foreland at the coast on the north [*Plafker*, 1987]. From these data it is clear that the 2° stratigraphic taper primarily reflects the northward thickening of the Yakataga Formation (Figure 6). Thus we assume that the preorogenic Kulthieth and Poul Creek Formations do not thicken appreciably across the study area.

[20] Together these data and assumptions form the basis of the deformed-state cross section, which was restored using a combination of line length and area balancing [*Mitra and Namson*, 1989; *Woodward et al.*, 1989]. Line lengths used included the top and bottom of the Yakataga and Poul Creek Formations and arbitrary intraformational markers. Line lengths and bed thickness are assumed constant within any thrust sheet. Because the depositional thickness of the Kulthieth Formation is not known, area of the Kulthieth Formation was conserved between the deformed and undeformed states assuming an undeformed thickness of 2800 m [*Mitra and Namson*, 1989]. Shortening at the structural level of the Kulthieth Formation has a large degree of uncertainty due to its uncertain thickness and pervasive deformation by faulting and folding [*Bruhn et al.*, 2004]. Shortening estimates at the structural level of the Kulthieth Formation depend on stratigraphic thickness because area is conserved between the deformed and undeformed states: A trade-off exists between shortening and thickness for any area balanced section wherein a greater or lesser amount of shortening are implied if the predeformational stratigraphic thickness is substantially less or more, respectively, than the assumed value. The line length restoration of the base of the Poul Creek and Yakataga Formations provide independent constraints on the restored area of the Kulthieth Formation.

[21] Restoration of the deformed-state section was based on matching hanging wall ramps and flats with their footwall counterparts for thrust sheets in which hanging wall cutoffs are preserved. Corresponding ramps and flats in the footwall are inferred from dip data and thrust sheet geometry [*Boyer and Elliott*, 1982; *Dahlstrom*, 1969]. Where hanging walls exposed at the surface have flat geometries, the hanging wall was restored to the base of the corresponding footwall ramp and the minimum shortening across the footwall measured [*Woodward et al.*, 1989]. These constraints limit the way in which surface geology can be extrapolated to depth, which eliminates structural interpretations that are not geometrically viable. The restored section can then be used to estimate the minimum shortening across the fold-and-thrust belt, illustrate the kinematic history, and constrain the magnitude of exhumation.

4.2. Major Structures and Architecture of the Yakutat Fold-and-Thrust Belt

[22] At least 6 major east-west trending thrust faults lie between the undeformed YT foreland offshore and the Chugach–St. Elias fault (Figure 3). The southernmost of these structures represent the frontal thrusts and are associated with submarine anticlines termed A1 and A2 (Figures 3, 6, and 7) [*Bruns and Schwab*, 1983]. In the migrated depth section of Bruns and Schwab, these faults are characterized as high-angle reverse faults (at least ~60°) with low displacement. Maximum offsets at "horizon C," a reflector at a stratigraphic depth of approximately 3 km within the Yakataga Formation, are ~500 m on A1 and ~1400 m on A2. Details of the fault geometry below the base of the Yakataga are unknown owing to a paucity of coherent reflectors at greater stratigraphic depths.

[23] Wells drilled into these anticlines encountered strata of the Yakataga and Poul Creek Formation. *Zellers* [1993] determined that the stratigraphic contact between the two units at the ARCO OCS Y-0007 well is unconformable, with deep water Oligocene deposits of the Poul Creek Formation overlain by mid-Pliocene glacial-marine shelf deposits of the Yakataga Formation. The major faults are interpreted to root into a décollement at the base of the Poul Creek Formation, which is consistent with fold/fault relationships and seismic data (Figure 6). Logs from the wells, which are extrapolated onto the section from along strike, report the possible presence of Kulthieth Formation, based on lithology, at an unknown depth. Thus, although our section infers a detachment at the base of the Poul Creek Formation, it is possible that the detachment is within the Kulthieth Formation.

[24] The next major structure to the north is the Sullivan fault and anticline, which are well exposed onshore as the southern front of the Robinson Mountains along the coast (Figure 3) [*Plafker*, 1987]. Along its length, the Sullivan fault juxtaposes Poul Creek Formation against the Yakataga Formation. In the vicinity of Yakataga Reef the structure changes orientation from WNW striking in the east to NE striking in the west, where it continues offshore as anticline A3 (Figure 3). On the northern flank of the Sullivan anticline, the Yakataga/Poul Creek depositional contact is exposed. At Yakataga Reef the contact is reported by *Lagoe* [1983] to be conformable, but an angular unconformity marks the contact in the Robinson Mountains [*Miller*, 1971]. On seismic line 406 growth strata geometries characterize the complete sequence of the Yakataga Formation in the southern limb of the Sullivan anticline, which indicates that the fold grew throughout deposition of the

unit after 5.6 Ma (Figure 7b). Well data from the Sullivan anticline indicate the presence of the Yakataga and Poul Creek Formations [*Plafker*, 1987]. Whether the Kulthieth Formation is present at depth in this structure is equivocal.

[25] On the basis of the thickness of the Poul Creek Formation exposed at this location, dip data, and structural geometry in line 406, we assume the Sullivan fault is a hanging wall flat within the Poul Creek Formation and a footwall ramp in the Yakataga Formation. A broad topographic low to the north of the Sullivan anticline, the White River Valley, marks the location of the White River Syncline (Figure 6). We infer that this regionally extensive structural low lies to the north of a footwall ramp-flat transition of the Sullivan fault (Figure 6).

[26] Steeply south-dipping Yakataga Formation strata define the north limb of the White River syncline, which is cut at the surface by the Miller Creek fault (Figure 3). We interpret this dip domain to form the southern limb of a regionally developed anticline, the Yakataga anticline, which can be traced along strike from the line of section east to Icy Bay (Figure 3). A thin strip of Kulthieth Formation is exposed in the hanging wall along the trace of the 70° north-dipping Miller Creek fault. Up-section stratigraphically from the Kulthieth Formation, a broad panel of generally north-dipping Poul Creek Formation is exposed and has been deformed by a series of minor folds. This north-dipping panel of rocks forms the south limb of the Leeper syncline (Figures 3 and 6). Poul Creek Formation is exposed in the core of the syncline, and the north limb is cut by the Hope Creek fault. Kulthieth Formation strata are juxtaposed against Poul Creek sediments across the Hope Creek fault [*Miller*, 1971].

[27] Strata in the hanging wall of the Miller Creek fault dip moderately to the north (Figure 6). In the region of the fault, however, Kulthieth and Poul Creek Formation strata in the hanging wall are steeply north dipping (Figure 3). Yakataga Formation in the footwall dips south. These observations suggest that the Miller Creek fault cuts an earlier-formed footwall anticline. In this interpretation, the region between the Sullivan and Hope Creek thrusts represents a single thrust sheet bifurcated by an out-of-sequence thrust. On the basis of this interpretation, a major ramp in the Yakataga Formation in the footwall of the Sullivan fault is inferred to project from the coast northward to beneath the Hope Creek fault (Figure 6). This model explains the high structural elevation of the Kulthieth and Poul Creek Formations relative to their subsurface depth in the foreland to the south in a region that is otherwise characterized by low dip (Figure 6).

[28] North of the Hope Creek fault, only Kulthieth Formation rocks are exposed across a broad belt extending to the Chugach–St. Elias fault. These rocks are strongly deformed by folding, faulting, and penetrative deformation, particularly adjacent to the Chugach–St. Elias fault [*Bruhn et al.*, 2004; *Miller*, 1971; *Plafker*, 1987; *Plafker et al.*, 1994b]. Rocks are dominantly north dipping from the Hope Creek fault to the Chugach–St. Elias fault [*Miller*, 1971]. North of the Hope Creek fault, some faults are recognized within the belt of Kulthieth Formation (i.e., the Kosakuts fault; Figures 3 and 6). Other faults (i.e., unnamed fault marked by question mark in Figure 3) are inferred from changes in strike and dip direction, from thrust sheet structural thickness, and from along-strike projection of mapped faults. A simple imbricate fan thrust system consisting of three imbricate thrust sheets is interpreted for the region between the Hope Creek and Chugach–St. Elias thrust faults. Assuming a 2800 m thickness for the Kulthieth Formation allows for a minimum estimate of shortening by the imbricate fan within the Hope Creek thrust. Penetrative deformation and internal folding between imbricate faults are not included in the shortening estimate. If the Kulthieth Formation is thinner, if additional imbricate faults are present, and if it were possible to account for penetrative deformation, the magnitude of internal shortening would be larger.

4.3. Structural Summary

[29] In summary, the YT fold-and-thrust belt consists of three major thrust sheets from north to south. The Hope Creek thrust sheet is the structurally highest thrust sheet and consists of a series of north-dipping imbricate thrust faults, exposes only the stratigraphically oldest Kulthieth Formation, and is bound on the north by the 40°–60° north dipping Chugach–St. Elias fault (Figures 3 and 9) [*Bruhn et al.*, 2004; *Estabrook et al.*, 1992]. Earthquakes on the plate boundary and on the Chugach/St. Elias fault in 1979 demonstrate their activity [*Estabrook et al.*, 1992]. A detachment near the base of the Kulthieth Formation for this thrust sheet is suggested by the fact that no older rocks are exposed along the fault traces. Emplacement of the Hope Creek thrust sheet is poorly constrained, but must have occurred after Poul Creek deposition (Figure 6). The Sullivan thrust sheet, extends from the Hope Creek thrust on the north to the Sullivan fault on the south. This second thrust sheet is cut by the Miller Creek fault. Whereas the oldest unit exposed along the Sullivan fault is the Poul Creek Formation, Kulthieth Formation occurs along the Miller Creek fault (Figures 3 and 6). A change in detachment depth from south to north, from the Poul Creek Formation to the Kulthieth Formation, respectively, is indicated by the difference in the oldest unit exposed along the Sullivan and Miller Creek faults (Figure 6). Decreasing dip up section and thinning of Yakataga Formation strata on the north end of seismic line 406, which is in the footwall of the Sullivan thrust, imply that motion on the Sullivan thrust was coeval with deposition after 5.6 Ma (Figure 7). A third thrust sheet comprises the two reverse faults offshore to the south of the Sullivan thrust (Figure 6). Offshore, well data and fold structural geometry suggest the décollement occurs near the base of the Poul Creek. Deformation migrated southward to fold A2, which formed after 1.8 Ma, and then to fold A1 after 0.25 Ma according to thickness changes of marker horizons across the crest of each anticline (Figure 7) [*Zellers*, 1995].

4.4. Shortening, Cross-Sectional Area, and Accretion

[30] Shortening was measured via line-length balancing of the deformed state cross section (Figure 6). Growth strata indicate fold growth associated with the Sullivan initiated prior to formation of the offshore folds (Figure 7). Thus,

individual structures were restored sequentially from south to north. Only minimum shortening can be measured from the cross section because the hanging wall cutoffs of all the major thrusts onshore are eroded. Roughly 82 km of shortening is recovered from restoration of the deformed state section of the thrust belt (Figure 6b). Contribution of individual thrust sheets to the shortening can also be determined. Horizontal translation ranges from a minimum of 29 km for the Sullivan thrust sheet (Figure 6a) to ~44 km for the Hope Creek thrust sheet (Figure 6). Seven kilometers of shortening are distributed between thrusts within the Hope Creek thrust sheet (Figure 6), the Miller Creek thrust, and the offshore structures A1 and A2. Rock uplift due to thrust fault displacement, using the deformed state as reference frame, which is characterized by a 2° stratigraphic taper, is a maximum of 7 km for the Sullivan thrust sheet and 15 km for the Hope Creek thrust sheet (Figure 6). If all the shortening in the thrust belt accumulated contemporaneously with Yakataga Formation deposition, the minimum long-term internal shortening rate is ~14 mm/a, or ~32% of the 44 mm/a modern convergence rate of Yakutat, in the foreland, with respect to North America [*Fletcher and Freymueller*, 1999; *Sauber et al.*, 1997].

[31] Shortening magnitude is impacted by several key interpretations. Stratigraphic location of the décollement, for example, steps up from the Kulthieth Formation to the base of the Poul Creek from north to south according to well data in the offshore and the oldest unit exposed in thrust sheets on shore (Figure 6). The combined observations that the Sullivan thrust has a similar dip to the strata in the hanging wall, the thrust sheet rocks are characterized by shallow north dips, and are elevated more than 7 km relative to the equivalent strata in the offshore to the south [*Miller*, 1957; 1971; *Plafker*, 1987], require location of the thrust sheet's footwall cutoff in the subsurface beneath the Hope Creek thrust to the north (Figure 6). Geometry of the Hope Creek thrust is inferred to be a hanging wall flat juxtaposed against a footwall flat. Whereas dip data permit this interpretation, it requires a large magnitude of shortening associated with emplacement of the thrust sheet. Although other interpretations are permissible, we favor the simple thrust sheet model because it is consistent with available surface and subsurface data, dip data, and stratigraphic thicknesses.

[32] A total cross-sectional area of 630 km^2 of YT sediments represents material in the actively deforming orogenic wedge; which is the thrust-bounded area above the basal décollement, south of Chugach–St. Elias fault, north of the southernmost thrust (at anticline A1) and below the topographic surface. Roughly 354 km^2 of sediment lie below the basal décollement between the foreland pin on the south and the Chugach–St. Elias fault to the north (Figure 6a). Maximum wedge thickness in the deformed state is ~15 km, measured from the highest topography to basal detachment. In the undeformed section, the stratigraphic section thickens from ~10 km in the undeformed foreland in the south to ~17 km in the north. The principal control of the undeformed-state stratigraphic taper is the syntectonic Yakataga Formation taper. It is assumed that the stratigraphic taper was lower and the depth of the Poul Creek and Kulthieth Formations was shallower prior to deposition of the Yakataga Formation.

5. Fission Track Dating

5.1. Background

[33] Fission track dating is commonly applied to apatite and zircon crystals to determine the time since cooling below an effective closure temperature of track retention. The cooling ages can be used to determine the amount of time a sample took to be exhumed through the upper crust, as well as place absolute age control on the events causing exhumation, provided the geothermal gradient was not perturbed by local and variable heat sources (i.e., local plutons). The method relies on the damage to crystal structure caused by the path of fission fragments that result from spontaneous fission of ^{238}U. During fission decay of ^{238}U, two highly charged nuclei repel from each other, producing a linear trail of damage (a fission track) [e.g., *Fleischer et al.*, 1975]. Fission track dating is similar to other radiometric dating systems, with a ^{238}U "parent" and fission track "daughter" product. At sufficiently high temperatures, fission tracks anneal as quickly as they are produced, but when cooled below a critical temperature that is specific to the mineral, tracks are retained and the system is closed. Track retention occurs within the partial annealing zone (PAZ), a range of temperatures within which tracks progressively anneal. In apatite, this zone is generally between ~60° and 110°C, and in zircon is between ~200° and 275°C, but like most thermochronometers, these temperatures are rate dependant and are slightly higher if cooling rates are rapid [e.g., *Brandon et al.*, 1998].

[34] Helium dating is based on the production of He within a crystal and the retention of He, which depends on temperature and crystal morphology. The critical temperatures for retention of He within apatite and zircon are ~70°C and ~180°C, respectively [*Reiners et al.*, 2002; *Wolf et al.*, 1996]. When FT and (U-Th)/He for apatite and zircon are combined, these chronometers constrain passage through 4 discrete isotherms within the upper ~10 km of the crust. A number of variables affect geothermal gradients in space and time including thrust fault motion, erosion, topographic evolution, and basin formation and other variables such as the cooling rate dependence on closure temperature [*Batt and Brandon*, 2002; *Brandon et al.*, 1998; *Brewer and Burbank*, 2006; *Ehlers and Farley*, 2003; *Garver et al.*, 2000; *House et al.*, 1998; *Mancktelow and Grasemann*, 1997; *Stüwe et al.*, 1994]. If a geothermal gradient for the crust is known then closure temperature can be translated to depth, and the cooling ages can be translated into the magnitude of exhumation and exhumation rates.

5.2. Detrital Sample Ages and Partial Resetting

[35] All samples taken from the YT in this study are from clastic sedimentary units that display little to no mineralogical evidence of metamorphism. Detrital fission track ages are unlike cooling ages of igneous rocks because each grain preserves the cooling history of its source terrain unless the

Table 1. Summary of Apatite Fission-Track Data[a]

Sample	E (m)	Latitude	Longitude	ρ_s	N_s	ρ_i	N_i	ρ_d	N_d	n	χ^2	Age	-1σ	$+1\sigma$	U ± 2se
YT, Unreset															
01–34a	579	60.2134°	142.6270°	1.66×10^5	63	2.29×10^6	869	3.626×10^6	5924	18	0.0	6.3	−1.2	1.4	25.1 ± 1.8
01–41a	274	60.0592°	141.9400°	4.77×10^5	107	2.65×10^6	594	3.691×10^6	6030	20	3.8	31.5	−3.4	3.8	28.6 ± 2.4
YT, Reset															
01–53a	1326	60.4181°	142.5119°	7.90×10^4	17	3.34×10^6	718	3.821×10^6	6243	19	0.0	3.4	−1.0	1.2	34.8 ± 2.7
02–31	1387	60.2855°	141.7640°	1.42×10^5	66	3.43×10^6	1593	3.887×10^6	6349	15	0.0	3.8	−0.8	0.9	35.1 ± 2.0
01–39a	297	60.2625°	143.3121°	1.26×10^5	20	3.95×10^6	625	3.669×10^6	5995	20	0.0	4.0	−1.1	1.3	42.8 ± 3.5
01–48a	1920	60.7911°	142.6368°	1.63×10^5	13	3.80×10^6	303	3.778×10^6	6172	13	0.0	5.0	−1.8	2.4	40.0 ± 4.7
01–29a	1082	60.2926°	142.3558°	1.00×10^5	12	3.13×10^6	375	3.560×10^6	5817	17	9.9	5.5	−1.6	2.0	35.0 ± 3.7
01–43a	279	60.1809°	141.1756°	1.07×10^5	23	1.56×10^6	337	3.713×10^6	6065	16	0.0	5.7	−1.8	2.3	16.7 ± 1.9
01–36a	883	60.3340°	142.6010°	5.84×10^4	10	1.77×10^6	303	3.647×10^6	5959	20	84.2	5.8	−1.9	2.4	19.3 ± 2.3
01–32a	442	60.3434°	142.4418°	9.29×10^4	13	2.60×10^6	364	3.604×10^6	5888	20	94.5	6.2	−1.8	2.2	28.7 ± 3.1
01–55	1204	60.1866°	141.0804°	1.21×10^5	77	7.71×10^5	492	3.865×10^6	6314	29	9.7	28.7	−3.5	4.0	7.9 ± 0.7
CT															
01–49a	2012	60.6793°	142.5340°	3.53×10^5	152	4.78×10^6	2059	3.800×10^6	6207	20	86.3	13.3	−1.2	1.3	50.0 ± 2.5
99–2	754	60.7203°	142.5435°	2.72×10^5	140	3.67×10^6	1885	3.908×10^6	6385	20	73.1	13.8	−1.3	1.4	37.4 ± 2.0
01–45a	1783	60.6572°	142.4146°	7.09×10^5	211	8.64×10^6	2572	3.734×10^6	6101	15	28.8	14.5	−1.2	1.3	92.2 ± 4.1
01–47a	1494	60.7672°	142.6065°	8.02×10^5	160	5.23×10^6	1043	3.756×10^6	6136	20	34.2	27.3	−2.5	2.7	55.4 ± 3.

[a]YT, Yakutat terrane; CT, Chugach terrane. Elevations are given in meters; ρ_s is the density (cm^2) of spontaneous tracks; N_s is the number of spontaneous tracks counted; ρ_i is the density (cm^2) of induced tracks; ρ_d is the density (cm^2) of tracks on the fluence monitor (CN1); n is the number of grains counted; χ^2 is the Chi-squared probability (%); and U is uranium concentration (ppm). Fission track ages ($\pm 1\sigma$) were determined using the Zeta method, and ages were calculated using the computer program and equations from *Brandon* [1992]. All ages with $\chi^2 > 5\%$ are reported as pooled ages; otherwise, χ^2 are shown. For apatite, a Zeta factor of 94.61 ± 4.16 (±1 SE − SJ) is based on determinations from both the Fish Canyon Tuff and the Durango apatite. Glass monitors (CN1 for apatite) placed at the top and bottom of the irradiation package were used to determine the fluence gradient. All samples were counted at 1250× using a dry 100× objective (10× oculars and 1.25× tube factor) on an Olympus BMAX 60 microscope fitted with an automated stage and a digitizing tablet.

rock has been reheated. The grain-age spectrum can generally be broken down into component populations characterized by grains with similar ages [*Brandon*, 1992]. Single grain ages and population ages are evaluated relative to the depositional age. A given grain age distribution can be older or similar to the depositional age (either unreset or partially reset), or younger than the depositional age (reset) of the stratigraphic unit [*Brandon*, 1992]. Discerning the degree of resetting requires an estimate of the depositional age range for a sample, which is particularly important for zircon (U-Th)/He and fission track chronometers because of the higher temperatures required for resetting these systems.

[36] Depending on the postdepositional temperature history of detritus, some or all of the grains may be reset with respect to a given thermochronometer. If all grains are reset, the mixture of initial grain ages is erased and all grains record a cooling event younger than the depositional age. Alternatively, if only some grains are reset, then the grain-age distribution will consist of multiple populations, where the youngest population represents the time of resetting and older populations that may or may not be related to source terrain cooling [*Garver et al.*, 2002]. Typically, the youngest peak is younger than the depositional age of the deposit and other peaks can be the same age as or older than the unit from which the grains were sampled. In such a sample, the youngest peak would be interpreted as a 'reset' age. If a component population overlaps a depositional age, the cooling age of the grain ages in this population is interpreted as related to a postdepositional heating event, possibly associated with sediment burial. Peaks that are older than the depositional age retain information about predeposition cooling in the source region, which can provided information about provenance, source-to-sink lag time, and other information about sediment production and transport [*Bernet and Garver*, 2005; *Cerveny et al.*, 1988; *Naeser et al.*, 1987].

[37] Partial resetting occurs when a group of grains within the sample are reset by a thermal event, whereas other, more retentive grains retain their older cooling ages. In apatite grains, the stability of fission tracks is largely a function of the Cl:Fl ratio and other aspects of apatite chemistry (see, for example, review by *Brandon et al.* [1998, and references therein]). Fluorapatite, in particular has the lowest track stability and accordingly, the lowest closure temperature (T_c).

[38] For zircon, the dominant factor affecting track stability is the amount of accumulated radiation damage [*Brandon et al.*, 1998; *Garver et al.*, 2005; *Kasuya and Naeser*, 1988]. Radiation damage results from both fission and α decay, although the greater frequency of α events makes it the more significant process in terms of creating radiation damage. Grains become increasingly disordered owing to α decay, which disrupts crystal structure. This disorder makes grains less retentive of fission tracks and also more chemically reactive (note section on sample etch times below). The amount of radiation damage a zircon has accumulated depends on the concentration of U and Th and time since original cooling of the crystal [*Garver et al.*, 2005]. Fission tracks in less retentive grains are less stable and reset at lower temperatures.

Table 2. Summary of Zircon Fission-Track Data[a]

Sample	Elevation	Latitude	Longitude	ρ_s	N_s	ρ_i	N_i	ρ_d	N_d	n	χ^2	Age	-1σ	$+1\sigma$	U ± 2se
99–2	754	60.7203°	142.5435°	4.92×10^6	885	7.96×10^6	1431	3.286×10^5	3874	14	1.0	34.4	−1.7	+1.8	297.9 ± 18.2
01–34	579	60.2134°	142.6270°	5.07×10^6	2288	5.78×10^6	2610	3.178×10^5	3746	32	0.0	39.6	−1.6	+1.7	223.8 ± 10.5
								3.190×10^5	3760					
01–36	883	60.3340°	142.6010°	4.57×10^6	1146	5.43×10^6	1363	3.166×10^5	3732	20	0.0	44.8	−2.0	+2.1	211.1 ± 12.6
01–41	274	60.0592°	141.9400°	6.65×10^6	1118	7.05×10^6	1185	3.010×10^5	3547	15	0.0	33.8	−2.0	+2.1	288.0 ± 18.1
01–48	1920	60.7911°	142.6368°	4.73×10^6	1334	4.25×10^6	1199	2.962×10^5	3490	21	0.0	48.4	−2.4	+2.6	176.7 ± 11.2
01–53	1326	60.4181°	142.5119°	4.80×10^6	2039	6.15×10^6	2615	2.914×10^5	3433	33	0.0	31.4	−1.4	+1.4	259.6 ± 12.5
								2.926×10^5	3490					
01–55	1204	60.1866°	141.0804°	5.22×10^6	1364	7.47×10^6	1950	2.878×10^5	3391	22	0.4	34.0	−1.5	+1.5	319.1 ± 17.5
02–31	1387	60.2855°	141.7640°	5.10×10^6	2251	6.12×10^6	2703	2.842×10^5	3348	37	0.0	37.3	−1.5	+1.5	264.9 ± 13.5
								2.854×10^5	3362					

[a]Elevations are given in meters; ρ_s is the density (cm^2) of spontaneous tracks; N_s is the number of spontaneous tracks counted; ρ_i is the density (cm^2) of induced tracks; ρ_d is the density (cm^2) of tracks on the fluence monitor (CN5); n is the number of grains counted; χ^2 is the Chi-squared probability (%); and U is uranium concentration (ppm). Fission track ages (±1se) were determined using the Zeta method, and ages were calculated using the computer program and equations from *Brandon* [1992]. All ages with $\chi^2 > 5\%$ are reported as pooled ages; otherwise, χ^2 ages are shown. For zircon, a Zeta factor of 348.45 ± 6.51 (±1 SE − SJ) is based on determinations from both the Fish Canyon Tuff and the Buluk tuff. Glass monitors (CN5) placed at the top and bottom of the irradiation package were used to determine the fluence gradient. All samples were counted at 1250× using a dry 100× objective (10× oculars and 1.25× tube factor) on an Olympus BMAX 60 microscope fitted with an automated stage and a digitizing tablet.

5.3. Laboratory Methods

[39] Apatite and zircon separates were prepared and analyzed following standard procedures for the external detector method [*Gleadow*, 1981; *Naeser*, 1976] (Tables 1 and 2). Apatite samples were mounted in thin section epoxy and etched in HNO_3 for 20 s to reveal fission tracks. Zircon samples were mounted in PFA Teflon and etched in a KOH:NaOH eutectic at 228°C. Two separate grain mounts were created for each zircon sample to allow for both a short and long etching. Different etch times are necessary for detrital suites because accumulated radiation damage (from α decay of ^{238}U and ^{232}Th) affects the chemical reactivity of zircon and varies greatly between individual grains. Because damage is largely a function of age, long etches are used to target young, hard to etch grains, whereas short etches reveal the older populations eradicated by the long-etch process [e.g., *Bernet and Garver*, 2005; *Garver and Kamp*, 2002; *Naeser et al.*, 1987]. For this study the long etches were 30 h and short etches ranged from 21 to 26 h. We generally focused on short-etch mounts for most samples.

[40] After etching, apatite and zircon grain mounts were fitted with low-U mica detectors and stacked along with age standards and uranium enriched glass dosimeters (CN1, CN5) in poly tubes. These packages were irradiated with thermal neutrons in the TRIGA reactor at Oregon State University at fluences of 8×10^{15} neutrons/cm^2 (apatite) and 2×10^{15} neutrons/cm^2 (zircon). Glass dosimeters placed at each end of the package are used to interpolate the neutron flux at each position in the package. Age standards used to calculate zeta calibration factors [*Hurford and Green*, 1983] include Durango fluorapatite and Fish Canyon Tuff for apatite, and Fish Canyon and Buluk Tuff for zircon. Zeta factors used are 94.61 ± 4.16 based on 10 analyses for apatite and 348.48 ± 6.51 based on 9 analyses for zircon (±1 standard error). For apatite samples, about 20 grains per sample were counted depending on the abundance of acceptable grains. For zircon samples between 14 and 37 grains were counted per sample.

5.4. Analysis of Sample Ages

[41] The χ^2 test was used to determine if individual grain ages for each sample belong to a single population [*Brandon*, 1992; *Galbraith*, 1981; *Green*, 1981]. Samples that pass the χ^2 test ($P(\chi^2) > 5\%$) are reported as pooled ages and samples that fail ($P(\chi^2) < 5\%$) are reported as χ^2 ages, which is the age of the youngest fraction of "plausibly related" grain ages [*Brandon*, 1992]. As expected for mixed detrital samples, all zircon samples failed the χ^2 test and ages reported in Table 2 are χ^2 ages. Peak fitting was thus used to deconvolve component populations (Table 3).

Table 3. Zircon Fission Track Binomial Component Ages[a]

Sample	Unit	Nt	P1 (Ma)	P2 (Ma)	P3(Ma)
01–34	Yakataga	32	34.1 Ma −2.6 +2.8 35.5%	51.0 Ma −3.7/+4.0 48.0%	100.4 Ma −9.5/+10.4 16.5%
01–41	Yakataga	15	38.0 Ma −2.1/+2.3 68.4%		113.5 Ma −12.2/13.7 31.6%
02–31	Poul Creek	37	34.4 Ma −1.9/+2.0 58.9%	53.4 Ma −3.7/+3.9 41.1%	
01–36	Poul Creek	20	41.2 Ma −2.4/+2.6 71.3%	66.8 Ma −7.2/+8.1 28.7%	
01–53	Kulthieth	33	26.4 Ma −2.0/+2.1 33.7%	41.9 Ma −2.6/+2.7 49.0%	68.4 Ma −5.9/+6.4 17.2%
01–55	Kulthieth	22	29.9 Ma −2.7/+2.9 55.0%	40.8 Ma −3.5/+3.8 45.0%	
01–48	Chugach	21	30.7 Ma −4.2/+4.9 15.6%	57.5 Ma −3.2/+3.4 73.2%	122.6 Ma −23.4/28.8 23.3%
99–2a	Chugach	14	28.2 Ma −3.6/+4.1 34.2%	39.6 Ma −3.1/+3.4 65.8%	

[a]Nt, number of dated grains; uncertainties cited at ±1 SE. Binomial component ages were determined using the BINOMFIT peak fitting program of *Brandon* [1992, 1996].

Peak ages were determined using a binomial peak-fitting routine (Binomfit of *Brandon* [1992]), which deconvolves grain ages into component Gaussian distributions, thereby preserving information about grain-age populations older than the youngest fraction [*Brandon*, 1992, 1996]. The youngest grain-age population is more conservatively estimated by the χ^2 age than the youngest grain-age population (P1) determined by peak-fitting methods. Statistically, it is ideal if the youngest peak age (P1) and the χ^2 age are similar.

6. Thermochronometry From the CSE

6.1. Apatite Fission Track Data

[42] Fission track ages were determined for a suite of samples across the width of the Yakutat fold-and-thrust belt

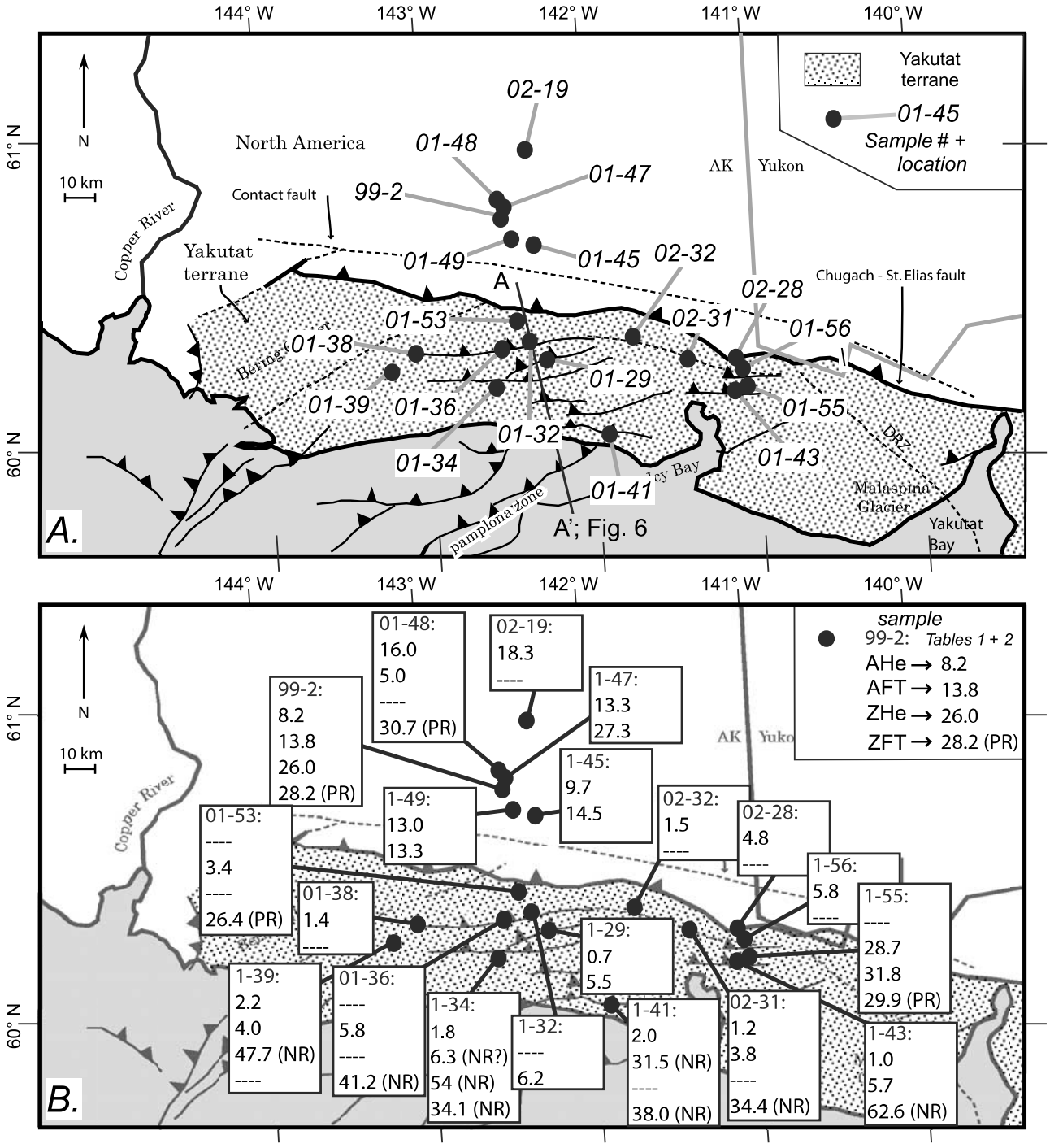

Figure 8

onshore and for metamorphic and plutonic rocks in the North American upper plate (Figures 8 and 9). In this study, 15 new apatite fission track ages (AFT) and 8 new zircon fission track ages were determined for the suite of samples measured by *Spotila et al.* [2004] for apatite and zircon (U-Th)/He (Figure 8 and Tables 1, 2, and 3). Ten new apatite fission track ages presented from YT sandstones/graywackes (Kulthieth, Poul Creek, Yakataga), and 5 samples are from Chugach terrane schists/phyllites, gneisses, and granitoids (Figure 8). Most of the samples have both apatite (U-Th)/He and fission track ages, and several also have zircon (U-Th)/He and fission track ages (Figure 8).

[43] Apatite FT ages for the 15 samples fall broadly into three groups (Table 1 and Figure 9b). The first group is represented by AFT ages that are significantly older than the depositional age of the unit sampled and thus clearly not reset. Sample 01CH41, for example, comes from the <5 to 6 Ma Yakataga Formation and has an AFT age of 31.5 Ma (−3.4/+3.8 Ma). This sample is from the flank of the Sullivan Anticline and is the sample closest to the coast (Figure 3). A second group of ages dominates the rest of the samples from the YT fold-and-thrust belt (Figure 9b). These ages range from 3.4 to 6.3 Ma, are consistently younger than the unit from which the sample was taken, and are thus reset with respect to depositional ages. A notable exception is sample 01CH55 (Kulthieth Formation) from the eastern part of the study area in the vicinity of Mt. St. Elias, which has an AFT age of 28.7 Ma (−3.5/+4.0 Ma). The AFT age is younger than (or very close to) the depositional age, but older than samples both in the upper plate of the Chugach/St. Elias fault and the YT fold-and-thrust belt (Figure 8). A third group of samples with like ages are from the upper plate of the Chugach/St. Elias thrust (Chugach terrane); ages range from 13.3 to 14.5 Ma (Figure 9b). Two samples from the upper plate, 01CH47 and 01CH48 are older (27.3 Ma), and younger (5.0 Ma), respectively, than the 13–14.5 Ma samples.

6.2. AFT Interpretation

[44] All samples have been reset with respect to apatite fission track closure at 110°C, with the exception of 01CH41, the sample from the Yakataga Formation in the Sullivan anticline near-coast (Figure 8). Several samples failed the χ^2 test (Table 1) suggesting that temperatures were in the 100° to 120° range, but not high enough to reset all grains [*Brandon et al.*, 1998]. The unreset sample from the Sullivan anticline (01CH41) likely reflects a shallow structural and stratigraphic position and/or thrust motion early in the Yakataga Formation accumulation history. Reset AFT samples from the YT are all 3.4 to 6.3 Ma, with no clear pattern to the distribution of ages (Figure 9b). Samples from the North American plate on the leeward flank of the range, although more variable, are mostly older, with a cluster of ages at 13–14 Ma, similar to the distribution of AHe ages (Figure 9a) [*Spotila et al.*, 2004]. AFT age data suggest that exhumation since 6 Ma has been greater on the southward, windward side of the range than in the North American upper plate to the north. Neither the age populations *within* the YT on the windward side of the range or within the upper plate on the leeward side, however, show a change of age with position. These two sample groups are distinguished by not only a contrast in climatic condition, but also a major terrane boundary. Both AHe and AFT data illustrate that over at least the last 5–6 Ma, the Yakutat terrane, on the windward side of the range, has experienced greater exhumation than the upper plate on the leeward side of the range.

6.3. Zircon Fission Track Data

[45] All zircon fission track (ZFT) data are presented in Tables 2 and 3. Six of the 8 samples dated by zircon fission track are from the YT (2 from each stratigraphic unit), and 2 are from the Chugach terrane (North America). Peak fitting methods were applied to the grain ages to determine component populations for each sample because all samples failed the χ^2 test. Zircon ages from the Yakataga Formation and Poul Creek Fm are older than the depositional ages and are therefore inferred to represent original cooling ages of the source rock (unreset). Each sample displays 2 to 3 age populations. Youngest peak ages (P1) for these two units range between 34.1 + 2.8/−2.6 Ma and 41.2 + 2.6/−2.4 Ma (Table 3). This age is substantially older than the depositional age (5.6 Ma to present) of the Yakataga Formation, indicating that these samples are neither reset, nor are the youngest peaks an approximation of the maximum depositional age. The fact that these grains are unreset is expected because the Yakataga Formation samples dated by AHe, AFT, and ZFT (01–34, 01–41; Tables 1 and 3) are unreset with respect to the lower temperature systems (Figure 8). Despite the wide range in possible Poul Creek Formation

Figure 8. (a) Simplified map of the study are showing sample locations of all apatite and zircon (U-Th)/He and fission track dates (Ma) used in this study. (b) Map of cooling ages listed in order of closure temperature (see key, upper right). Dashes indicate that no age has been determined for a particular chronometer, and boxes with only two ages or less indicate that dates were obtained from apatite systems only. (U-Th)/He ages are from *Spotila et al.* [2004]. Three of these ages have been updated with additional replicates [*Berger and Spotila*, 2006]. New (U-Th)/He age determinations are 0.7 ± 0.11 Ma for 01–29, 1.8 ± 0.59 Ma for 01–34, and 2.0 ± 0.54 Ma for 01–41. The original age determinations for these samples were inaccurate and imprecise owing to high blanks and insufficient number of replicate analyses. The revised average ages are based on approximately five replicates per sample, which, combined with updated analytical procedures, yields more reliable and accurate results. All other (U-Th)/He ages are unchanged from *Spotila et al.* [2004]. All ages are interpreted to be reset except where noted as "NR" (not reset) or "PR" (partially reset). Zircon fission track ages include only the youngest peak age (Table 3). The extent of the onshore Yakutat terrane is indicated by the stipple pattern. DRZ is the Dangerous River zone.

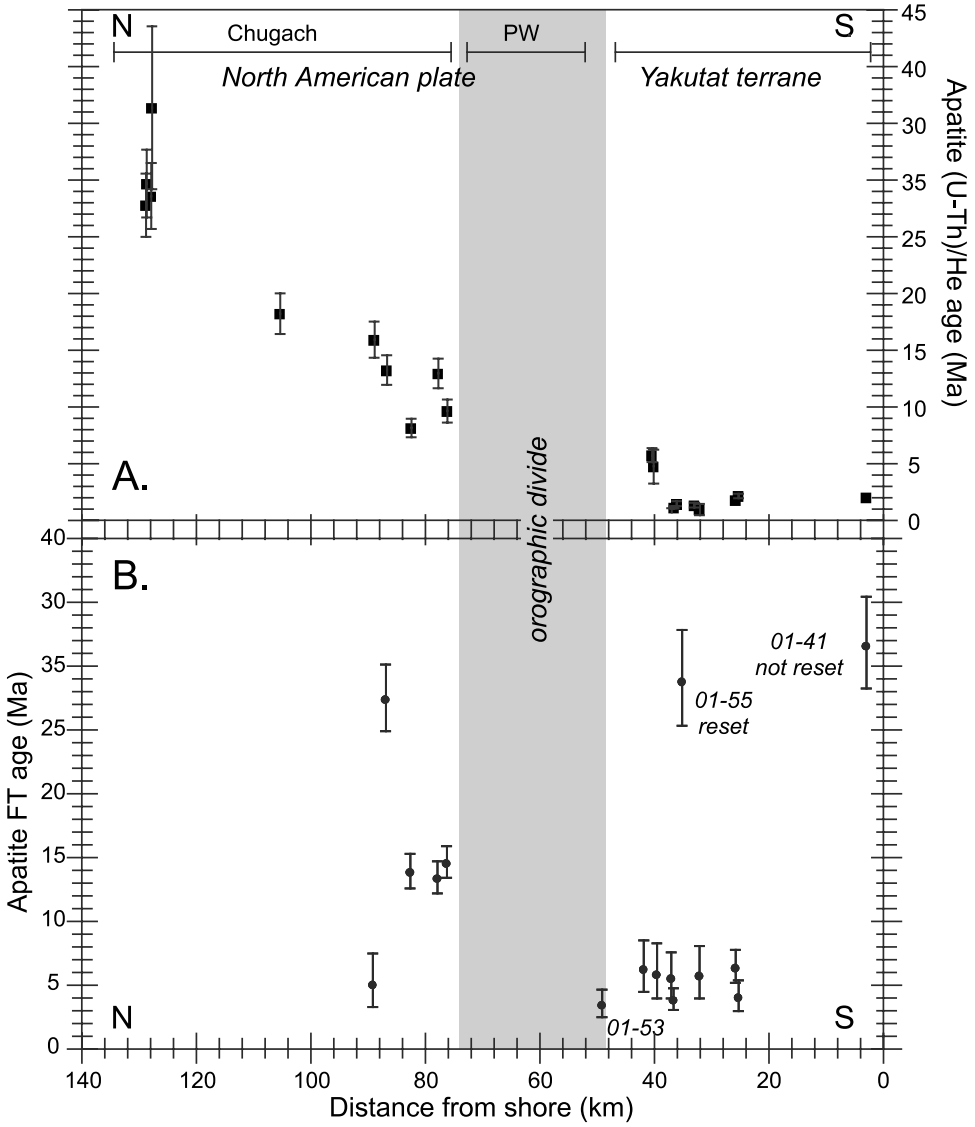

Figure 9. (a) Apatite (U-Th)/He ages (±2σ) plotted with distance from the coast (0 km) (modified from *Spotila et al.* [2004] and *Berger and Spotila* [2006]). Location of terranes is indicated. Note that the orographic divide is located roughly 60 km north of the coast. (b) Apatite fission track ages (±1σ) plotted with distance from the coast (see Figure 8 and Table 1).

depositional ages (as young as latest Miocene or old as Oligocene, see Figure 4) the youngest peaks for these samples (02−31, 01−36; Table 3) are older than the depositional age. Thus the Poul Creek Formation samples are unreset with respect to ZFT, but unlike the Yakataga Formation samples, are reset with respect to AHe and/or AFT. A second age population (P2) at 51.0−66.8 Ma is recorded by both the Yakataga and Poul Creek samples. The third population (P3) is present only in Yakataga Fm samples and is 100.4−113.5 Ma (Table 3).

[46] ZFT population distributions from the Kulthieth Formation samples are more ambiguous, largely because of the poor control on the depositional age. Youngest peak (P1) ages for Kulthieth Formation samples are 26.4 + 2.1/−2.0 (01−53) and 29.9 +2.9/−2.7 Ma (01−55). The depositional age of the Kulthieth Formation and related Tokun Formation are ∼48−35 Ma according to *Plafker* [1987] (Figure 4); the maximum age estimates for the Kulthieth Formation and equivalents range from Early Eocene to Early Oligocene (∼55−28.5 Ma) [*Plafker*, 1987; *Plafker et al.*, 1994b]. Thus, depending on the upper bound on depositional age, the P1 ages are within error of deposition, and may be unreset like other foreland samples. In this case, we would interpret the Kulthieth samples much the same as the Yakataga and Poul Creek samples, where P1, P2 and P3 are a series of age populations inherited from the original source area. This source, however, would have zircons with cooling ages that are essentially equal to the youngest depositional age, a characteristic indicative of a volcanic source [*Garver et al.*, 2000].

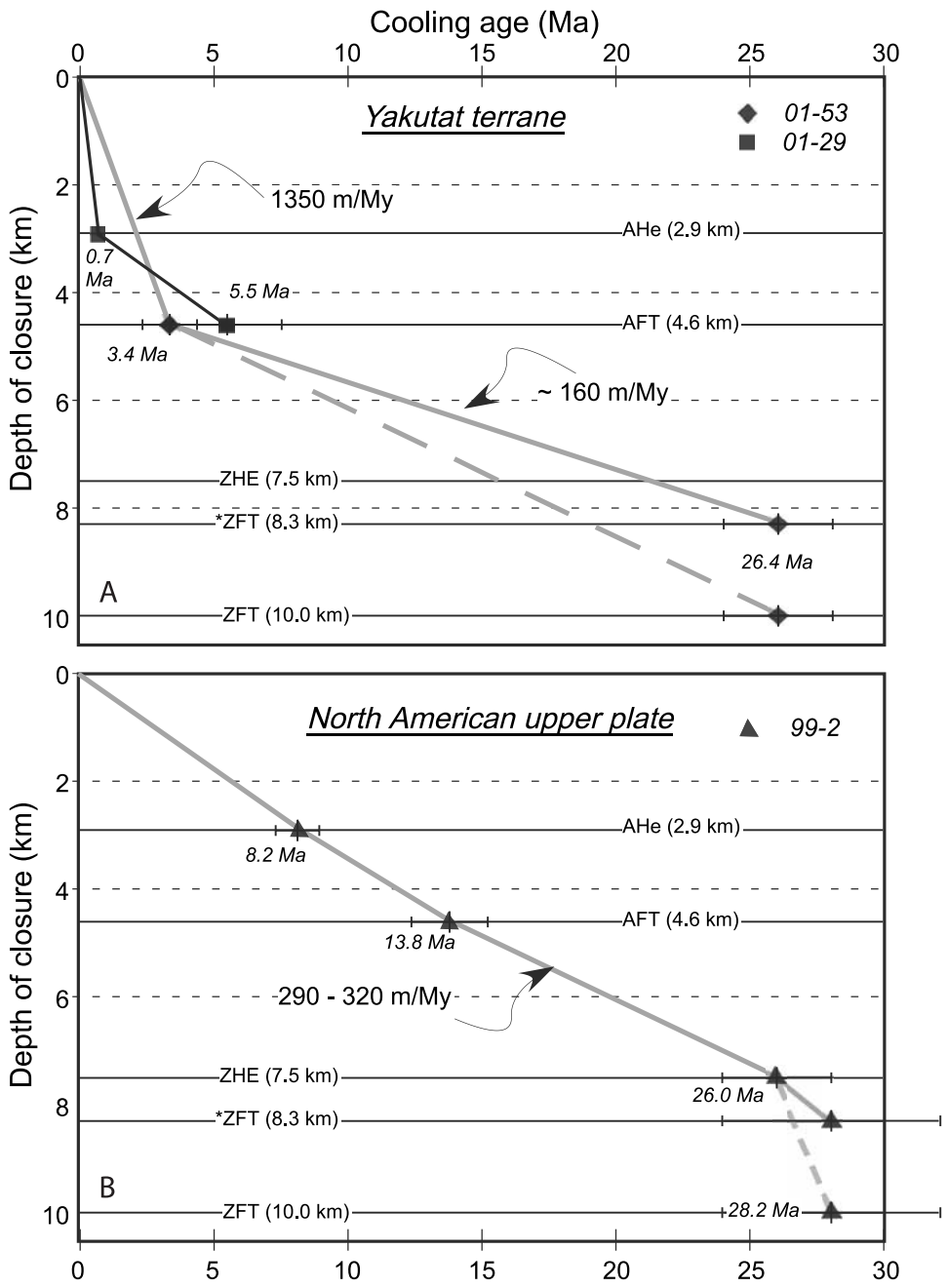

Figure 10. Plots of age versus depth for samples from the (a) Yakutat terrane (samples 01–29 and 01–53, Kulthieth Formation, Figure 8 and Tables 1 and 2) and (b) Chugach terrane (sample 99CH2, North American upper plate, Figure 8 and Tables 1 and 2). Slow cooling characterizes the period from 26 to 5 Ma. Between 5 and 0 Ma, cooling rate accelerated in the Yakutat terrane while the rate remained unchanged in the North American upper plate. A 24° ± 5°C/km geothermal gradient is used to convert closure temperatures to depth. A ±0.2 km error is assigned to each depth, which is equivalent to the size of the symbols. Age uncertainties are indicated and reported in Tables 1 and 2. Dashed line shows cooling path for non-α-damaged zircon, which has a higher closure temperature than α-damaged zircon [*Garver et al.*, 2005].

[47] A second possibility is that the Kulthieth samples have been partially reset. In this case, the P1 peaks at 26.4–29.9 Ma represent the time of cooling above the zircon PAZ, as recorded by only the least retentive grains [see *Garver et al.*, 2005]. If the samples are partially reset, the significance of P2 and P3 (~41 Ma and 68 Ma respectively) is ambiguous, because these peaks could consist of zircons that have retained their source area ages throughout the

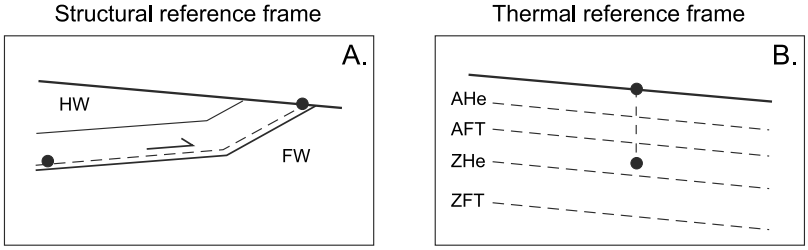

Figure 11. (a) Sketch of a simple thrust fault to illustrate net rock motion that can be derived from geologic structure. Note that the reference frame of particle motion is the hanging wall (HW) and footwall (FW) strata with no constraint on the location of the surface. (b) Motion of a particle toward the surface as recorded by thermochronometers. In the thermal reference frame, motion of rock is at high angles to isotherms, and provides no information on particle motion parallel to isotherms. Isotherm shape and spacing is a function of erosion rate and topography [e.g., *Ehlers and Farley*, 2003; *House et al.*, 1998; *Mancktelow and Grasemann*, 1997; *Stüwe et al.*, 1994].

partial resetting thermal event, or they also represent some unknown degree of partial resetting. Complete resetting is not likely given the existence of multiple peak ages.

[48] The two samples from the Chugach terrane (01CH48, 99–2) also contain peaks of multiple ages. Both are located within amphibolite facies rocks of the Chugach metamorphic complex, that formed from thermal events associated with ridge-trench interactions between ~54 and 48 Ma [e.g., *Bradley et al.*, 2003; *Sisson et al.*, 1989; *Sisson et al.*, 2003]. *Sisson et al.* [1989] documented a maximum metamorphic temperature range from ~400°C to ~650°C across the complex from its edge to the highest-grade gneissic core. Sample 99–2 is a gneiss collected east of the Tana Glacier, near Granite Creek, and is thus located within the high-grade core (schist and gneiss zone of *Hudson and Plafker* [1982]). Sample 01CH48, a schist-phyllite was collected farther north, near the transition between the highest-grade core and the intermediate, or schist zone of *Hudson and Plafker* [1982]. The intermediate zone is also amphibolite facies and 01CH48 is well within a zone of minimum temperatures of 400°C [*Sisson et al.*, 1989].

6.4. ZFT Interpretation

[49] Zircon fission track ages are largely unreset for YT samples with the potential exception of Kulthieth Formation samples 01–53 and 01–55, which are interpreted as being partially reset. Whether or not these samples have been partially reset has important consequences for our interpretation of original sample depth. Published vitrinite reflectance values of 0.37% to 3.41% for Kulthieth Formation samples indicate maximum temperatures of ~44°C to ~275°C [*Barker*, 1988; *Johnsson et al.*, 1992]. These data were used to compile the Thermal Maturity Map of Alaska, which has very extensive sample coverage within the study area [*Johnsson and Howell*, 1996]. Temperatures indicated for outcrops of the Kulthieth Formation toward the rear of the wedge, near the Chugach–St. Elias fault, are all greater than 200°C and as high as 272°C. These values are sufficient to reset radiation-damaged zircons [*Garver et al.*, 2005]. Sample 01–55 may be an example of a population that includes damaged zircons. The minimum zircon FT age peak is similar to the sample's ZHe, and AFT ages and to the youngest possible age of the Kulthieth Formation (Early Oligocene), which suggests the thermochronometers record a depositional age. If the Kulthieth Formation is no younger than ~35 Ma [*Plafker*, 1987], then the minimum ZFT, the ZHe, and the AFT ages are reset and record a postdepositional cooling event at ~32–29 Ma (Figure 8). If correct, the grains probably experienced temperatures of 180° to 200°C [*Garver et al.*, 2005].

[50] Chugach terrane samples clearly record cooling events at 31–28 Ma, at ~40–57.5 Ma, and an older event (Table 3). Some of the apatite data also record the ~30 Ma event (Figure 8), which may have been widespread. A 54–48 Ma metamorphic event [*Bradley et al.*, 2003; *Sisson et al.*, 1989, 2003] may be recorded by P2 (sample 01–48; 57.5 Ma), although P2 from sample 99–2 is 39.6 Ma (Table 3).

6.5. Geothermal Gradient

[51] Paleogeothermal gradient for the YT is estimated by combining three approaches. Vitrinite reflectance data sampled in offshore well OCS-Y-211 (star, Figure 2) [*Johnsson and Howell*, 1996; *Plafker*, 1987], was converted to temperature using $T(°C) = 148 + 104[\ln(R_m)]$ on the basis of the mean vitrinite reflectance values (R_m) [*Barker*, 1988]. Vitrinite reflectance from this well suggests a 24.6°C/km geothermal gradient from 2.2 to 4.4 km depth. Heat flow in the only 2 wells within a distance of 2° latitude and 5° longitude of Icy Bay used to construct the Alaska portion of the Geothermal Map of North America (points GC and Tanana, see the database http://www.smu.edu/geothermal/georesou/alaska.htm), were used to calculate a geothermal gradient [*Blackwell and Richards*, 2004]. No wells with measurements are available for the study area. Geothermal gradient ranges from 21° ± 4°C/km to 25° ± 5°C/km given the range in heat flow values (50 to 55 mW/m^2) and thermal conductivities (2 to 3 W/m/°K) in the wells. Taking the 50–64 mW/m^2 range of heat flow values reported on the Geothermal Map of Alaska for the southern flank of the Chugach/St. Elias Range [*Blackwell and Richards*, 2004] and a thermal conductivity range of 2 to 3 W/m/°K yields a

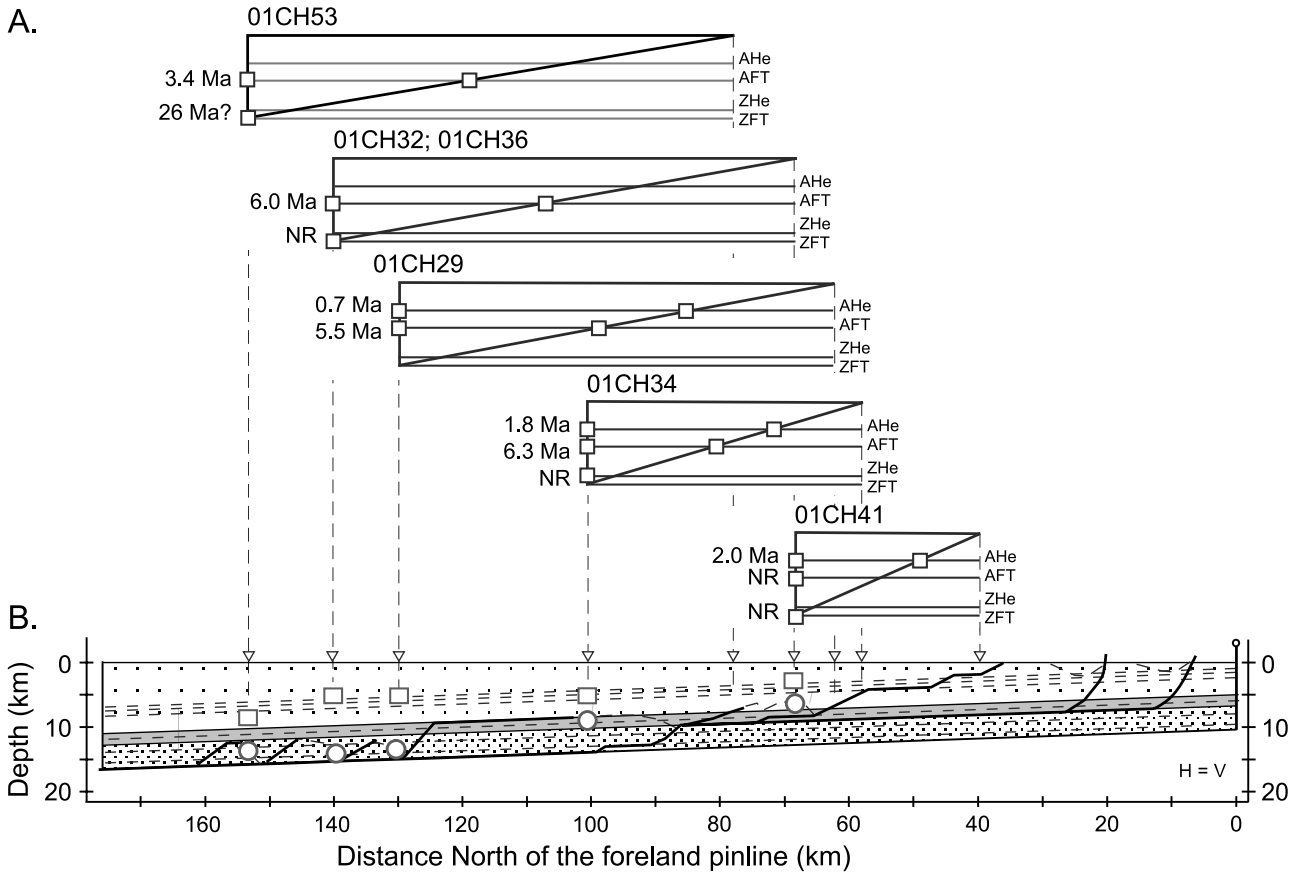

Figure 12. Sample cooling age (Figure 8) as a function of structural position in the restored state (Figure 6). (a) For each sample shown, the left end of the right triangle is the restored state position of a given sample, the right end is the current sample location in the deformed state (triangles), and the vertical axis shows the mineral (box) and cooling age for each sample (thermochronometers (track retention/closure depths in kilometers) are AHe (2.9), AFT (4.6), ZHe (7.5), and α-damaged ZFT (8.3) and 24°C/km geothermal gradient). The vertical axis of the triangle is vertically exaggerated 1.5 times. Boxes on the hypotenuse of each triangle represent the location that each sample crossed a critical isotherm for closure of the thermochronometer for a linear path described by the maximum depth of burial, the restored structural position, and the present structural position at the surface. (b) Circles mark the sample location in the restored state. Note that the maximum depth constrained by the thermochronometric data (boxes) is consistently shallower than the position implied by the structural restoration.

geothermal gradient that changes from 21° ± 4°C/km at the coast to 26° ± 5°C/km in the core of the range. An average geothermal gradient of 24° ± 5°C/km is used on the basis of the available data.

[52] Cooling recorded by a given thermochronometer can be translated to amount of exhumation by converting temperature to depth. A 24°C/km geothermal gradient places AHe closure at 2.9 km, AFT at 4.6 km, ZHe at 7.5 km, and ZFT at 7.5–8.3 km (using Tc = 180°–200°C for α-damaged zircon; [*Garver et al.*, 2005]). A 5°C/km error is equal to a 0.2 km error for each converted depth value. A higher geothermal gradient shifts the closure to shallower depths and a lower gradient implies greater closure depths. Using the assumptions of low-amplitude topography and a 24°C/km geothermal gradient, the thermochronometric data indicate maximum depths of burial for the samples are consistently shallower than their positions in the restored-state cross section (Figures 12 and 13). Whereas the assumptions of a constant geothermal gradient with depth, that modern heat flow approximates heat flow at the time cooling, and that low-relief topography characterizes the thermal structure at depth are inherently simplistic [*Reiners and Brandon*, 2006], direct measurements of heat flow from the study area do not exist, paleotopography at the time of cooling is unconstrained, and available data do not constrain if and when a steady state thermal structure was established in the orogen. Given these unknowns, we

chose to treat the thermal structure in the orogen at the time of cooling conservatively.

6.6. Integration of AHe, AFT, ZHe, and ZFT Thermochronometric Data

[53] Data from multiple thermochronometers can be used to constrain time-temperature history of samples, exhumation rates in time, and restoration depths of thrust sheets. Combining AHe, AFT, ZHe, and ZFT thermochronometric data allows for ~8–10 km of the motion of rock with respect to the surface to be constrained at 4 points in time (Figure 10). Comparison of the highest-temperature mineral/thermochronometric system that is reset (i.e., AFT = 110°C) with the lowest temperature mineral/system that is not reset (i.e., ZHe = 180°C) brackets the maximum temperature for a given sample, which serves as a proxy for the restored depth of thrust sheets. Most of the zircon (U-Th)/He and zircon fission track samples are not reset and therefore postdepositional exhumation rates can only be determined from the apatite data (upper ~4 km) for most of the samples. Combined AHe and AFT data are generally complementary (Figure 9), although the AHe cooling rate is nominally faster in some cases.

[54] The few samples that do have reset ZHe ages or partially reset ZFT ages merit discussion, however, because their longer cooling histories record changes in exhumation rate and show a contrast between the YT and North American upper plate cooling. For example, sample 01–53, a Kulthieth Formation sample from the northern edge of the YT, can be inferred to record relatively slow cooling (160 m/My) between ZFT closure at 26.4 Ma and AFT closure at 3.4 Ma, followed by faster cooling between 3.4 Ma and the present (1350 m/My; Figure 10a). This faster cooling from ~3–6 Ma to the present is typical of most YT samples (i.e., 01–29, Figure 10a). Sample 99–2, from the North American upper plate (Chugach terrane), also records a period of slow cooling (290–320 m/My) starting at 28.2 Ma. Unlike the YT samples, the slow rate continues through AFT and AHe closure to the present (Figure 10b). Acceleration in exhumation rate after 6 Ma, assuming a constant geothermal gradient, is seen in YT apatite samples from the windward flank of the range, but is not seen in the North American upper plate samples from the leeward flank of the range (Figures 8 and 10b).

[55] With the exception of sample 01–53 (and possibly 01–55), none of the samples from the YT are reset with respect to either the zircon (U-Th)/He or zircon fission track systems. The fact that they are not reset is a meaningful observation because these data constrain wedge geometry (maximum thickness). Thus, the rocks in the footwall of the Chugach/St. Elias thrust at the rear of the wedge have not been heated to temperatures greater than 180°C, the top of the ZFT partial annealing zone (ZPAZ). If sample 01–53 is partially reset, the maximum postdepositional temperature would have been very close to the ZPAZ, as the sample has been heated enough to lower its ZFT age, but have not been enough to anneal all tracks, as burial below the PAZ would do. For a geothermal gradient of 24°C/km, this suggests exhumation from 7 to 8 km (Figure 10), which is comparable to the depth of the basal décollement in the footwall of the Chugach/St. Elias thrust in the deformed state cross section (Figure 6a).

7. Discussion

7.1. Structural and Thermochronologic Constraints on Sample Paleodepth and Position

[56] One of the goals of incorporating a structural model with thermochronometric data is to put one-dimensional exhumation data into a two-dimensional context (horizontal and vertical position within a wedge). Used alone, thermochronometers provide a one-dimensional estimate of exhumation at each individual sample location (Figure 11) [*Reiners and Brandon*, 2006]. When used in conjunction with the restored position of the thrust sheets from which they were sampled, the ratio of horizontal to vertical motion with respect to the Earth's surface and the net eroded area for the thrust belt can be determined. Sample cooling rate is influenced by both absolute changes in exhumation rate and by particle path relative to isotherms [e.g., *Batt and Brandon*, 2002]. For example, a rock that moves up at a shallow angle with respect to isotherms will record a slower cooling history than a package of rock that moves at a high angle relative to isotherms (Figure 11). For this reason, changes in cooling rate can reflect either an absolute change in exhumation rate or be due to a change in the trajectory of rock with respect to the surface in the face of a constant exhumation rate (Figures 10 and 12).

[57] Eroded area can be measured from the cross section from the missing area between the northward projection of the youngest Yakataga Formation in the foreland and the top of the preserved rock in the restored state cross section (Figure 13a). The eroded area in this frame of reference is 1150 km^2. The magnitude of northward thickening of the Yakataga Formation (above thrust sheets 2–5) is the principal control on the structurally constrained paleodepth of the northernmost samples. If thrusting occurred after the onset of Yakataga Formation deposition at ~5.6 Ma, this estimate places an upper bound on the maximum exhumation.

[58] The distribution of reset samples provides a second way to measure total exhumation off the top of the wedge (Figure 13b). On the south, at the coast, sample 01CH41 from the Sullivan anticline indicates the least burial, because only the AHe system is reset (Figures 3, 8, and 9). This sample was thus buried to depths between 2.9 and 4.6 ± 0.2 km (Figure 12). All samples are reset with respect to AHe and AFT across the wedge to the north (Figures 9 and 12 and Table 1). Neither ZHe nor ZFT are reset for the same samples (Figure 8 and Table 2). ZFT may be partially reset in samples 01–53 and 01–55 at the rear of the YT in the footwall of the Chugach/St. Elias thrust (Figures 9 and 12), which suggests these are radiation damaged zircons implying a maximum burial depth of 7.5 to 8.3 ± 0.2 km. The maximum depth of burial of the rear of the wedge is difficult to constrain, however, because the samples likely include zircon grains without radiation damage, for which Tc could be as high as 300°C (or 12.5 km for a 24°C/km geotherm) [*Garver et al.*, 2005]. Thus, the front of the

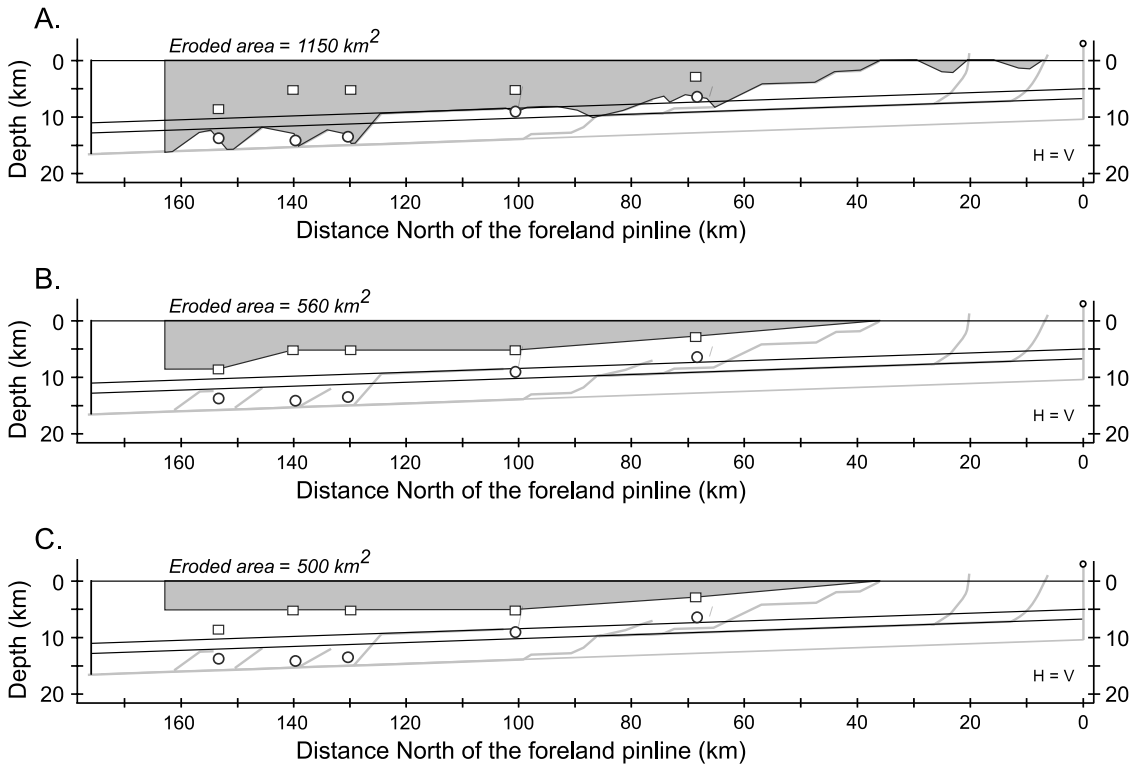

Figure 13. (a) Estimate of total eroded area removed from the Yakutat fold-and-thrust belt based on cross-section restoration and stratigraphic taper. (b) Estimate of total eroded area from restored cross section and thermochronometric depth constraints. (c) Estimate of area eroded during the last ~6 Ma based on cross-section restoration and thermochronology.

onshore wedge was buried to depths of 2.9 to 4.6 km and the rear of the wedge may have been buried to depths of 7.5–8.3 km (Figure 12). Total exhumation since 26 Ma (the oldest reset ZFT cooling age) is roughly 560 km^2 (Figure 13b), which is less than the exhumation predicted by the structural model (Figure 13a).

[59] A third way to think about exhumation is to consider the exhumation over the timescale of internal shortening and foreland basin development. Given that the base of the Yakataga Formation is 5.6 Ma [*Lagoe et al.*, 1993], exhumation over the last ~6 Ma occurred contemporaneously with foreland basin development. Erosional removal of ~500 km^2 since 6 Ma is constrained by 6 Ma and younger AFT and AHe cooling ages (Figures 8 and 13c). No more than ~7 km of material was removed from the most Hope Creek thrust sheet, the internal thrust sheet (Figure 6), according to these data. The eroded area tapers to less than 4.6 km at the leading edge of the Sullivan thrust sheet (Figure 13c). Cooling between 6 and 1.8 Ma was accompanied by distributed internal deformation given that the Sullivan anticline grew throughout Yakataga Formation deposition (Figure 7). Deformation stepped southward offshore into the undeformed foreland after anticline A1 began growing after 1.8 Ma (Figure 7b).

7.2. Convergence, Shortening Rate, and Exhumation

[60] The cross section indicates that the fold and thrust belt in the Yakataga area has undergone a minimum of ~82 km of margin-normal shortening, or about 51% shortening. One context in which this number can be evaluated is via comparison with the convergence of Yakutat with respect to North America, which is unknown but can be estimated as 240 km for last 6 Ma using the present GPS velocity [*Fletcher and Freymueller*, 1999; *Sauber et al.*, 1997]. Eighty two kilometers of shortening is a minimum estimate of the total shortening because nearly all the hanging wall cutoffs of the thrust sheets are eroded and penetrative deformation is not constrained. If the 82 km of shortening accumulated over the last 6 Ma, a ~13–14 mm/a convergence rate of the hanging wall of the Chugach/St. Elias thrust with respect to the undeformed Yakutat foreland is implied. These rates are predicated on the assumption that all the shortening was coeval with Yakataga Formation deposition. Whether internal shortening within the YT occurred prior to the onset of Yakataga Formation deposition is not known. A well in the Gulf of Alaska has ~10 Ma detritus inferred to have been sourced from the Chugach/St. Elias Range, an observation which is used to infer that the range had a topographic expression by ~10 Ma [*Lagoe et al.*, 1993]. Our rates compare well with those inferred from

map reconstructions of the relative motion of the YT with respect to North America [*Pavlis et al.*, 2004]. On the assumption that the majority of the shortening accumulated after 6 Ma, internal deformation within the YT fold-and-thrust belt accounts for 34% of the motion of the Yakutat block with respect to North America. Motion of YT with respect to North America not accounted for by the cross section must be absorbed by some combination of subduction of the YT without accretion, internal, distributed deformation within the YT, strike-slip motion on the Contact and other faults, and far-field deformation in the North American plate [*Lahr and Plafker*, 1980; *Mazzotti and Hyndman*, 2002; *Pavlis et al.*, 2004].

[61] Three simple thrust sheets accommodated the fault-related motion of YT with respect to North America (Figure 3). Minimum displacement on the major faults decreases from 44 km for the Hope Creek thrust sheet, to 35 km for the Sullivan thrust sheet, and 3 km for the folds in the foreland offshore to the south (Figure 6). Within the Sullivan thrust sheet, more displacement is associated with the Sullivan fault (27 km) than with the Miller Creek fault (8 km). Both the Miller Creek and Sullivan faults cut the Yakataga Formation and growth strata in the footwall of the Sullivan thrust (Figures 6 and 7), which argues that emplacement of the Sullivan thrust sheet initiated after 6 Ma. A minimum shortening rate of ~5–6 mm/a for the Sullivan thrust sheet, parsed between 1.3 mm/a on the Miller Creek fault and 4.5 mm/a on the Sullivan fault, can be inferred from the displacements on the faults and the age for the base of the Yakataga Formation. Timing and amount of shortening on the offshore fold/fault pairs can be derived from the cross section (Figure 6) and growth strata across each fold (Figure 7). Fold A2 accounts for 1.6 km of shortening and began growing after 1.8 Ma, implying a 0.9 mm/a average shortening rate. Fold A1 defines the deformation front within the YT separating the undeformed foreland to the south from the fold-and-thrust belt to the north (Figures 3 and 6). About the same amount of shortening (1.4 km) is represented by A1 as by A2, but A1 is younger than 0.25 Ma (Figure 7), which implies a higher shortening rate (5.6 mm/a). A high sedimentation rate combined with an earlier and slower slip rate on the A1 fold would mask fold growth prior to 0.25 Ma. No data constrain the timing of emplacement of the Hope Creek thrust sheet. If the shortening rate within the YT fold-and-thrust belt has been relatively steady since 6 Ma, these data imply that active shortening persisted on the Hope Creek thrust sheet as deformation migrated into the undeformed foreland basin to the south.

[62] Exhumation amount and rate can be compared both across the fold-and-thrust belt and across the Sullivan and Hope Creek thrust sheets. AHe and AFT data indicate that exhumation rates are between ~0.3 and 4 mm/a. Each of the onshore thrust sheets shows distinctive exhumation rate patterns. For example, Yakataga Formation samples in the Sullivan thrust sheet within 15 km of the cross section are not reset with respect to AFT (samples 01CH41 and 34; Figures 3 and 8). A sample from the Poul Creek Formation, in contrast (01CH29), has reset AFT and AHe ages, which implies that exhumation rate increased from 0.3 ± 0.1 km/Ma between 5.5 and 0.7 Ma to 4 ± 1.8 km/Ma after 0.7 Ma (Figure 10a). An order of magnitude rate increase likely reflects a change from a low-angle to a high-angle trajectory of rock with respect to the isotherms due to translation across a footwall flat to ramp transition after 0.7 Ma (Figure 11), although an increase in the geothermal gradient associated with an acceleration in erosion rate cannot be ruled out. Samples adjacent to the cross section from the Hope Creek thrust sheet include O1CH32, 36, and 53 from south to north, respectively (Figure 3). Whereas these samples suggest exhumation rates comparable to those from the deep parts of the Sullivan thrust sheet, the cooling through the AFT partial annealing zone occurred later (3.4 ± 1.1 Ma) and therefore at a faster rate (1.3 ± 0.2 mm/a) for sample 01CH53 (Figure 10a). Locally high rates (>1.5 ± 1 mm/a) are also recorded by cooling ages of samples distributed along the strike length and in the hanging wall of the Hope Creek fault (01CH38, 02CH31, and O2CH32; Figures 3 and 8). Thus, vertically averaged exhumation rates are ~20% of the shortening rates for the onshore thrust sheets, which is expected for a fold-and-thrust belt because horizontal particle motions are typically much larger than vertical motions (Figure 11) [*Batt and Brandon*, 2002; *Boyer*, 1992, 1995].

7.3. Pliocene Climate Change, Sediment Fluxes, and Exhumation

[63] Average sediment accumulation rates of the Yakataga Formation change from 0.17 mm/a between 5.6 and 4.2 Ma to 1.8 mm/a between 4.2 and 3.5 Ma to 4 mm/a between 3.5 and 2.6 Ma [*Zellers*, 1993]. The post 5.6 Ma sedimentation rate increase is concomitant with the appearance of dropstones in the Yakataga Formation, which is interpreted to reflect he onset of alpine glaciation in the Chugach/St. Elias Range [*Eyles et al.*, 1991; *Lagoe et al.*, 1993; *Miller*, 1953; *Plafker and Addicott*, 1976]. An increase in sedimentation rates between 4 and 2 Ma deduced from a global compilation of records from marine and nonmarine basins suggests a geomorphic disequilibrium on the continents resulting from oscillations between glacial and interglacial climates [*Zhang et al.*, 2001]. Accelerated rates of cooling and exhumation between 6 and 3 Ma in the Chugach/St. Elias thrust belt (Figure 10) and accelerating rates of sedimentation in the Yakataga foreland over the same time interval may be a reflection of sustained geomorphic disequilibrium due to the presence of glaciers, the tidewater setting of the windward side of the range, and an oscillating climate, which is well documented on shorter timescales in Icy Bay [*Meigs et al.*, 2006]. In detail, however, exhumation rate changes are closely related with individual thrust sheets (compare samples 01–53 and 01–29, Figure 10a). Encroachment of the thrust belt on the foreland basin due to the southward migration of thrusting and the thrust load represents an alternative explanation for the increased foreland sediment accumulation rate [*Brozovic and Burbank*, 2000].

7.4. What is the 'State' of Accretion, Shortening, Exhumation, and Topography?

[64] Within error, most of the AFT and AHe data across the thrust belt give similar cooling ages (Figure 9), which

indicate that the Chugach/St. Elias Range is in an exhumational steady state [*Willett and Brandon*, 2002] or that the exhumation rate is high enough that there is less spatial variability in cooling ages [*Ehlers and Farley*, 2003]. In detail the fact that relatively few samples have paired AFT and AHe analyses makes it difficult to demonstrate that the orogen experienced steady exhumation after ~5 Ma (Figure 10a). Moreover, exhumation rate varies according to structural position. The highest rates are closely associated with the hanging wall of Hope Creek thrust (Figure 8). In the Sullivan thrust sheet, samples from the structurally and stratigraphically deep Poul Creek Formation are reset whereas the relative shallow Yakataga Formation samples are unreset. Thus the pattern of exhumation is not solely a function of the structural evolution of the orogen [*Willett and Brandon*, 2002], but closely follows position within the stratigraphic succession and relative to fault ramps and flats.

[65] A comparison between the cross-sectional area of the fold-and-thrust belt in the deformed state (Figure 6a) and the eroded area as determined from the restored state cross section, the total exhumation, and the exhumation since ~6 Ma (Figure 13) provide a range of measures to compare the tectonic influx with the erosional efflux. Roughly 630 km^2 of material are within the orogenic wedge between the Chugach/St. Elias fault on the north and the A1 fault on the south (Figure 6a). If the undeformed material in the footwall of the basal décollement are included, the total cross-sectional area of the wedge is ~870 km^2. Given that the amount of eroded material based on the undeformed cross section is inconsistent with the thermochronometric data, this estimate is an absolute maximum. Total exhumation is ~560 km^2 since ~26 Ma, the oldest partially reset ZFt age (Figure 13 and Table 3). Since ~6 Ma, the exhumation off the top of the wedge has been ~500 km^2 (Figure 13). When viewed on the ~30 Ma timescale, the influx and efflux approach one another. At the timescale of the last 6 Ma, the influx exceeds the efflux by ~40%. More detailed knowledge of the timing and the variation of rate of thrusting in space and time, however, are critical to understanding the degree to which the exhumation is paced by the tectonic influx. It is interesting to note that the total material in the wedge doubled after 1.8 Ma when the faults of A2 and then A1 became active. This addition of material occurred without concomitant exhumation to the south of the Sullivan fault. Exhumation continued to the north, as evidenced by AHe cooling ages less than 2 Ma (Figure 8). Thus, although this analysis is consistent with arguments for a flux steady state [*Spotila and Meigs*, 2004], the influx has been episodic in part and varies owing to thrust front propagation into the undeformed foreland.

[66] The strong gradient in orographic precipitation across the CSE allows for comparison with the predictions of coupled erosion-deformation models. Apatite (U-Th)/He and fission track data indicate that rates and magnitudes of exhumation have been greater on the windward side of the orogen, within the Cenozoic sediments of the Yakutat terrane, for at least the last 5–6 Ma. AHe data show a clear trend of increasing age with distance from the coast, which can be attributed to more intensive erosion due to the extensive glacial cover and lower regional ELA toward the coast [*Berger and Spotila*, 2006; *Meigs and Sauber*, 2000; *Spotila et al.*, 2004]. The new AFT data presented here demonstrate a similar trend (Figure 9). Exhumation and crustal shortening are focused on the windward side of the range, which is characterized by younger cooling ages and higher exhumation rates. It is important to note that in the study area, the orographic divide closely parallels the major terrane boundaries between the Yakutat and Prince William/Chugach terranes (Figures 2 and 4). The thermochronometric data do not uniquely distinguish, however, between an orographically controlled erosion signal and a signal related to the different tectonic and deformational history of the terranes. For example, it is possible that exhumation after 6 Ma within the YT is in response to the propagation of deformation southward from the terrane boundary and that the Chugach terrane in the upper plate became increasingly isolated from the locus of active rock uplift. If this migration of deformation was accompanied by substantial building of topography, which is not known, focused erosion on the windward flank creates positive feedback that localizes the tectonic influx (Figure 1) [*Willett*, 1999]. In this scenario, the leeward flank of the wedge, the Chugach terrane north of the orographic divide, becomes less active with respect to both erosion and deformation.

8. Summary and Conclusions

[67] 1. Structure within the Yakutat fold-and-thrust belt is divided along three principal thrust sheets that are younger from north to south. The principal thrust sheets are the Hope Creek, Sullivan, and an unnamed thrust sheet offshore from north to south, respectively.

[68] 2. The basal décollement of the thrust belt steps upsection from ~17 km depth in the Kulthieth Formation on the north to ~7 km depth in the Poul Creek Formation on the south.

[69] 3. A minimum of ~82 km of shortening has been absorbed by the fold-and-thrust belt (53% shortening).

[70] 4. Minimum displacement on the major thrust sheets decreases from 44 km for the Hope Creek thrust sheet, to 35 km for the Sullivan thrust sheet, and 3 km for the offshore thrust sheet.

[71] 5. Sullivan thrust sheet emplacement was coeval with Yakataga Formation deposition, which began at 5.6 Ma. The ''offshore'' thrust sheet comprises the two reverse fault/fold pairs offshore to the south of the Sullivan fault (Figure 6). Fold A2 on the north formed after 1.8 Ma and fold A1 to the south formed after 0.25 Ma. Emplacement of the Hope Creek thrust sheet occurred coeval with or after deposition of the Poul Creek Formation.

[72] 6. If the 82 km of shortening accumulated over the last 6 Ma, a ~13–14 mm/a convergence rate of the hanging wall of the Chugach/St. Elias thrust with respect to the undeformed Yakutat foreland with the YT is implied. Average horizontal shortening rate of the Sullivan thrust sheet is 5–6 mm/a and increase from ~1 to ~6 mm/a between 1.8 and 0.25 Ma for the offshore thrust sheet.

[73] 7. The cross sectional area of the deformed orogenic wedge is 630 km^2.

[74] 8. Apatite fission-track ages for the CSE fall generally into three groups: unreset samples at the coast, reset samples in the YT that cooled below AFT closure at 6–3 Ma, and reset samples from the backstop that cooled at ~13 Ma. The difference between YT and backstop AFT cooling may be due to heavier precipitation and erosion on the windward side of the orogen, or could reflect exhumation in response to a young phase of rock uplift captured only in the Yakutat terrane.

[75] 9. All zircon fission-track samples have multiple peak ages. Only the most internal rocks of the YT are potentially partially reset. Samples from the backstop also have multiple peak ages, which is surprising given the metamorphic temperatures these rocks were exposed to.

[76] 10. AHe and AFT data indicate that exhumation rates are between ~0.5 and 4 mm/a.

[77] 11. Total exhumation estimates vary from 1150 km^2 on the basis of the restored cross section, 560 km^2 on the basis of the a partially reset zircon fission-track sample at the rear of the wedge, to 500 km^2 on the basis of apatite thermochronometers that have 6 Ma and younger ages.

[78] 12. Particle trajectories through the orogen, as constrained by both structure and thermochronology, have large horizontal components relative to the vertical motions, suggesting that sample cooling may have occurred over average paths that are nonvertical and controlled by fault geometry.

[79] 13. The CSE matches several predictions of coupled erosion-deformation models of a "wet prowedge" system including greater exhumation on the windward side, a locus of the most deeply exhumed rocks on the windward side of the orogen interior, a lack of erosion and deformation on the leeward side, and relatively shallow particle trajectories through the orogen. However, the data do not uniquely distinguish between orographically versus tectonically controlled erosion.

[80] **Acknowledgments.** Research was supported by NSF grant EAR-0001192 and NASA grant NASA (NAG-5-7646). Steve Reese and the OSU Triga Radiation Center are thanked for irradiation of our samples. Ron Bruhn is thanked for discussions. Associate Editor Margie Rusmore and reviewers Don Fisher and Todd Ehlers provided thoughtful reviews of the manuscript. Danny Rosenkrans and Devi Sharp of the Wrangell/St. Elias Park and Preserve were instrumental in facilitating this work.

References

Andrews, J. T. (1972), Glacier power, mass balances, velocities, and erosion potential, *Z. Geomorphol.*, *13*, 1–17.

Barker, C. E. (1988), Geothermics of petroleum systems: Implications of the stabilization of kerogen thermal maturation after a geologically brief heating duration at peak temperature, *U. S. Geol. Surv. Bull.*, *1870*, 26–29.

Barros, A. P., and D. P. Lettenmeir (1994), Dynamic modeling of orographically induced precipitation, *Rev. Geophys.*, *32*, 265–284, doi:10.1029/94RG00625.

Batt, G. E., and M. T. Brandon (2002), Lateral thinking: 2-D interpretation of thermochronology in convergent orogenic settings, *Tectonophysics*, *349*, 185–201, doi:10.1016/S0040-1951(02)00053-7.

Beaumont, C., et al. (1992), Erosional control of active compressional systems, in *Thrust Tectonics*, edited by K. R. McClay, pp. 1–18, Chapman Hall, New York.

Berger, A. L., and J. A. Spotila (2006), Strain partitioning within the western Chugach-St. Elias orogen, Alaska: The effect of glacial erosion, *Geol. Soc. Am. Abstr. Programs*, *38*, 450.

Bernet, M., and J. I. Garver (2005), Fission-track analysis of detrital zircon, *Rev. Mineral. Geochem.*, *58*, 205–237, doi:10.2138/rmg.2005.58.8.

Blackwell, D. D., and M. Richards (2004), Geothermal map of North America, map, Am. Assoc. of Petrol. Geol., Tulsa, Okla.

Boyer, S. E. (1992), Geometric evidence for synchronous thrusting in the southern Alberta and northwest Montana thrust belts, in *Thrust Tectonics*, edited by K. R. McClay, pp. 377–390, Chapman and Hall, London.

Boyer, S. E. (1995), Sedimentary basin taper as a factor controlling the geometry and advance of thrust belts, *Am. J. Sci.*, *295*, 1220–1254.

Boyer, S. E., and D. Elliott (1982), Thrust systems, *Am. Assoc. Pet. Geol. Bull.*, *66*, 1196–1230.

Bradley, D., et al. (2003), Geologic signature of early Tertiary ridge subduction in Alaska, in *Geology of a Transpressional Orogen Developed During Ridge-Trench Interaction Along the North Pacific Margin*, edited by V. B. Sisson et al., pp. 19–49, Geol. Soc. of Am., Boulder, Colo.

Brandon, M. T. (1992), Decomposition of fission-track grain-age distributions, *Am. J. Sci.*, *292*, 535–564.

Brandon, M. T. (1996), Probability density plots for fission-track grain-age samples, *Radiat. Meas.*, *26*, 663–676, doi:10.1016/S1350-4487(97)82880-6.

Brandon, M. T., et al. (1998), Late Cenozoic exhumation of the Cascadia accretionary wedge in the Olympic Mountains, northwest Washington State, *Geol. Soc. Am. Bull.*, *110*, 985–1009, doi:10.1130/0016-7606(1998)110<0985:LCEOTC>2.3.CO;2.

Brewer, I. D., and D. W. Burbank (2006), Thermal and kinematic modeling of bedrock and detrital cooling ages in the central Himalaya, *J. Geophys. Res.*, *111*, B09409, doi:10.1029/2004JB003304.

Brozovic, N., and D. W. Burbank (2000), Dynamic fluvial systems and gravel progradation in the Himalayan foreland, *Geol. Soc. Am. Bull.*, *112*, 394–412, doi:10.1130/0016-7606(2000)112<0394:DFSAGP>2.3.CO;2.

Brozovic, N., et al. (1997), Climatic limits on landscape development in the northwestern Himalaya, *Science*, *276*, 571–574, doi:10.1126/science.276.5312.571.

Bruhn, R. L., et al. (2004), Deformation during terrane accretion in the Saint Elias orogen, Alaska, *Geol. Soc. Am. Bull.*, *116*, 771–787, doi:10.1130/B25182.1.

Bruns, T. R. (1983), Model for the origin of the Yakutat block, an accreting terrane in the northern Gulf of Alaska, *Geology*, *11*, 718–721, doi:10.1130/0091-7613(1983)11<718:MFTOOT>2.0.CO;2.

Bruns, T. R., and P. R. Carlson (1987), Geology and petroleum potential of the southeast Alaska continental margin, in *Geology and Petroleum Potential of the Continental Margin of Western North America and Adjacent Ocean Basins-Beaufort Sea to Baja California*, edited by D. W. Scholl et al., pp. 269–282, Circum-Pac. Counc. for Energy and Miner. Resour., Houston, Tex.

Bruns, T. R., and W. C. Schwab (1983), Structure maps and seismic stratigraphy of the Yakataga segment of the continental margin, northern Gulf of Alaska, *U. S. Geol. Surv. Misc. Field Stud. Map*, *MF-1424*.

Cerveny, P. F., et al. (1988), History of uplift and relief of the Himalaya over the past 18 Ma: Evidence from fission-track ages of detrital zircons from sandstones of the Siwalik Group, in *New Perspectives in Basin Analysis*, edited by K. Kleinspehn and C. Paola, pp. 43–61, Univ. of Minn. Press, Minneapolis.

Dahlen, F. A. (1990), Critical taper model of fold-and-thrust belts and accretionary wedges, *Annu. Rev. Earth Planet. Sci.*, *18*, 55–99, doi:10.1146/annurev.ea.18.050190.000415.

Dahlstrom, C. D. A. (1969), Balanced cross sections, *Can. J. Earth Sci.*, *6*, 743–757.

Davis, D., et al. (1983), Mechanics of fold-and-thrust belts and accretionary wedges, *J. Geophys. Res.*, *88*, 1153–1172, doi:10.1029/JB088iB02p01153.

DeCelles, P. G., and G. Mitra (1995), History of the Sevier orogenic wedge in terms of critical taper models, northeast Utah and southwest Wyoming, *Geol. Soc. Am. Bull.*, *107*, 454–462, doi:10.1130/0016-7606(1995)107<0454:HOTSOW>2.3.CO;2.

DeMets, C., et al. (1994), Effect of recent revisions to the geomagnetic reversal time scale on estimates of current plate motions, *Geophys. Res. Lett.*, *21*, 2191–2194, doi:10.1029/94GL02118.

Eberhart-Phillips, D., et al. (2006), Imaging the transition from Aleutian subduction to Yakutat collision in central Alaska, with local earthquakes and active source data, *J. Geophys. Res.*, *111*, B11303, doi:10.1029/2005JB004240.

Ehlers, T. A., and K. A. Farley (2003), Apatite (U-Th)/He thermochronometry: Methods and applications to problems in tectonic and surface processes, *Earth Planet Sci. Lett.*, *206*, 1–14, doi:10.1016/S0012-821X(02)01069-5.

England, P., and P. Molnar (1990), Surface uplift, uplift of rocks, and exhumation of rocks, *Geology*, *18*, 1173–1177, doi:10.1130/0091-7613(1990)018<1173:SUUORA>2.3.CO;2.

Estabrook, C. H., et al. (1992), Tectonic model of the Pacific-North America plate boundary in the Gulf of Alaska from broadband analysis of the 1979 St. Elias, Alaska earthquake and its aftershocks, *J. Geophys. Res.*, *97*, 6587–6612, doi:10.1029/92JB00131.

Eyles, C. H., et al. (1991), The Yakataga Formation; A late Miocene to Pleistocene record of temperate glacial marine sedimentation in the Gulf of Alaska, in *Glacial Marine Sedimentation: Paleoclimatic Significance*, edited by J. B. Anderson and G. M.

Ashley, pp. 159–180, Geol. Soc. of Am., Boulder, Colo.

Fleischer, R. L., et al. (1975), *Nuclear Tracks in Solids: Principles and Techniques*, 605 pp., Univ. of Calif. Press, Berkeley.

Fletcher, H. J., and J. T. Freymueller (1999), New GPS constraints on the motion of the Yakutat block, *Geophys. Res. Lett.*, *19*, 3029–3032, doi:10.1029/1999GL005346.

Galbraith, R. F. (1981), On statistical models for fission-track counts, *J. Math. Geol.*, *13*, 471–478, doi:10.1007/BF01034498.

Garver, J. I., and P. J. J. Kamp (2002), Integration of zircon color and zircon fission-track zonation patterns in orogenic belts: Application to the Southern Alps, New Zealand, *Tectonophysics*, *349*, 203–219, doi:10.1016/S0040-1951(02)00054-9.

Garver, J. I., et al. (2000), Towards a more complete record of magmatism and exhumation in continental arcs, using detrital fission-track thermochronometry, *Phys. Chem. Earth*, *25*, 565–570, doi:10.1016/S1464-1895(00)00086-7.

Garver, J. I., et al. (2002), Partial resetting of fission tracks in detrital zircon, paper presented at International Workshop on Fission-Track Analysis: Theory and Applications, Soc. Geol. de España, Cadiz, Spain.

Garver, J. I., et al. (2005), Implications for timing of Andean uplift from thermal resetting of radiation-damaged zircon in the Cordillera Huayuash, Northern Peru, *J. Geol.*, *113*, 117–138, doi:10.1086/427664.

Gleadow, A. J. W. (1981), Fission-track dating methods: What are the real alternatives?, *Nucl. Tracks*, *5*, 3–14, doi:10.1016/0191-278X(81)90021-4.

Green, P. F. (1981), A new look at statistics in fission-track dating, *Nucl. Tracks*, *5*, 77–86, doi:10.1016/0191-278X(81)90029-9.

Gulick, S. P., et al. (2007), Geophysical insights into the Transition fault debate: Propagating strike slip in response to stalling Yakutat block subduction in the Gulf of Alaska, *Geology*, *35*, 763–766, doi:10.1130/G23585A.1.

Hallet, B., et al. (1996), Rates of erosion and sediment evacuation by glaciers: A review of field data and their implications, *Global Planet. Change*, *12*, 213–235, doi:10.1016/0921-8181(95)00021-6.

House, M. A., et al. (1998), Dating topography of the Sierra Nevada, CA, using apatite (U-Th)/He ages, *Nature*, *396*, 66–69, doi:10.1038/23926.

Hudson, T., and G. Plafker (1982), Paleogene metamorphism of an accretionary flysch terrane, eastern Gulf of Alaska, *Geol. Soc. Am. Bull.*, *93*, 1280–1290.

Humphrey, N. F., and C. F. Raymond (1994), Hydrology, erosion, and sediment production in a surging glacier: Variegated glacier, *J. Glaciol.*, *40*, 539–552.

Hurford, A. J., and P. F. Green (1983), The zeta age calibration of fission-track dating, *Isot. Geosci.*, *1*, 287–317.

Johnsson, M. J., and D. G. Howell (1996), Generalized thermal maturity map of Alaska, *U. S. Geol. Surv. Misc. Geol. Invest. Map*, *I-2494*, 1 p.

Johnsson, M. J., et al. (1992), Vitrinite reflectance and conodont color alteration index data from Alaska: Data to accompany the thermal maturity map of Alaska, in *U. S. Geol. Surv. Open File Rep., 92–409*.

Kasuya, M., and C. W. Naeser (1988), The effect of a-damage on fission-track annealing in zircon, *Nucl. Tracks Radiat. Meas.*, *14*, 477–480, doi:10.1016/1359-0189(88)90008-8.

Koons, P. O. (1990), Two-sided orogens: Collision and erosion from the sandbox to the Southern Alps, New Zealand, *Geology*, *18*, 679–682, doi:10.1130/0091-7613(1990)018<0679:TSOCAE>2.3.CO;2.

Koppes, M., and B. Hallet (2002), Influence of rapid glacial retreat on the rate of erosion by tidewater glaciers, *Geology*, *30*, 47–50, doi:10.1130/0091-7613(2002)030<0047:IORGRO>2.0.CO;2.

Lagoe, M. B. (1983), Oligocene through Pliocene foraminifera from the Yakataga Reef section, Gulf of Alaska Tertiary Province, Alaska, *Micropaleontology*, *29*, 202–222, doi:10.2307/1485567.

Lagoe, M. B., et al. (1993), Timing of late Cenozoic tidewater glaciation in the far North Pacific, *Geol. Soc. Am. Bull.*, *105*, 1542–1560, doi:10.1130/0016-7606(1993)105<1542:TOLCTG>2.3.CO;2.

Lahr, J. C., and G. Plafker (1980), Holocene Pacific-North American plate interaction in southern Alaska: Implications for the Yakataga seismic gap, *Geology*, *8*, 483–486, doi:10.1130/0091-7613(1980)8<483:HPAPII>2.0.CO;2.

Mancktelow, N. S., and B. Grasemann (1997), Time-dependent effects of heat advection and topography on cooling histories during erosion, *Tectonophysics*, *270*, 167–195, doi:10.1016/S0040-1951(96)00279-X.

Mayo, L. R. (1986), Annual runoff rate from glaciers in Alaska: A model using the altitude of glacier mass balance equilibrium, in *Cold Regions Hydrology Symposium*, edited by D. L. Kane, pp. 509–517, Am. Water Resour. Assoc., Bethesda, Md.

Mazzotti, S., and R. D. Hyndman (2002), Yakutat collision and strain transfer across the northern Canadian Cordillera, *Geology*, *30*, 495–498, doi:10.1130/0091-7613(2002)030<0495:YCASTA>2.0.CO;2.

Meigs, A., and J. Sauber (2000), Southern Alaska as an example of the long-term consequences of mountain building under the influence of glaciers, *Quat. Sci. Rev.*, *19*, 1543–1562, doi:10.1016/S0277-3791(00)00077-9.

Meigs, A., et al. (2006), Ultra-rapid landscape response and sediment yield following glacier retreat, Icy Bay, southern Alaska, *Geomorphology*, *78*, 207–221, doi:10.1016/j.geomorph.2006.01.029.

Miller, D. J. (1953), Late Cenozoic marine glacial sediments and marine terraces of Middleton Island, Alaska, *J. Geol.*, *61*, 17–40.

Miller, D. J. (1957), Geology of the southeastern part of the Robinson Mountains, Yakataga District, Alaska, *U. S. Geol. Surv. Oil Gas Invest. Map*, *187*, 2 pp.

Miller, D. J. (1971), Geology of the Yakataga District, Gulf of Alaska Tertiary Province, *U. S. Geol. Surv. Misc. Invest. Map, 61-102*, 2 pp.

Mitra, S., and J. S. Namson (1989), Equal area balancing, *Am. J. Sci.*, *289*, 563–599.

Naeser, C. W. (1976), Fission-track dating, *U. S. Geol. Surv. Open File Rep.*, *76-190*, 65 pp.

Naeser, N. D., et al. (1987), Provenance studies by fission-track dating of zircon-etching and counting procedures, *Nucl. Tracks Radiat. Meas.*, *13*, 121–126, doi:10.1016/1359-0189(87)90022-7.

O'Sullivan, P. B., and L. D. Currie (1996), Thermotectonic history of Mt. Logan, Yukon Territory, Canada, *Earth Planet. Sci. Lett.*, *144*, 251–261, doi:10.1016/0012-821X(96)00161-6.

Palmer, A. R., and J. Geissman (1999), Geologic time scale, report, 1 pp., Geol. Soc. of Am., Boulder, Colo.

Pavlis, T. L., et al. (2004), Tectonic processes during oblique collision: Insights from the St. Elias orogen, northern North American Cordillera, *Tectonics*, *23*, TC3001, doi:10.1029/2003TC001557.

Péwé, T. L. (1975), *Quaternary Geology of Alaska*, *U. S. Geol. Surv. Prof. Pap.*, *835*, 145 pp.

Plafker, G. (1987), Regional geology and petroleum potential of the northern Gulf of Alaska continental margin, in *Geology and Petroleum Potential of the Continental Margin of Western North America and Adjacent Ocean Basins-Beaufort Sea to Baja California*, edited by D. W. Scholl et al., pp. 229–268, Circum-Pac. Counc. for Energy and Min. Resour., Houston, Tex.

Plafker, G., and W. O. Addicott (1976), Glaciomarine deposits of Miocene through Holocene age in the Yakataga Formation along the Gulf of Alaska margin, in *Recent and Ancient Sedimentary Environments in Alaska*, edited by T. P. Miller, pp. Q1–Q23, Anchorage Geol. Soc., Anchorage, Alaska.

Plafker, G., and D. J. Miller (1958), Glacial features and surficial deposits of the Malaspina District, Alaska, *U. S. Geol. Surv. Open File Rep.*, *57–91*, 13 pp.

Plafker, G., et al. (1982), Holocene marine terraces and uplift history in the Yakataga seismic gap near Icy Cape, Alaska, *U. S. Geol. Surv. Circ.*, *844*, 111–115.

Plafker, G., et al. (1994a), Neotectonic map of Alaska, in *The Geology of Alaska*, edited by G. Plafker and H. C. Berg, Plate 12, 1 p., Geol. Soc. of Am., Boulder, Colo.

Plafker, G., et al. (1994b), Geology of the southern Alaska Margin, in *The Geology of Alaska*, edited by G. Plafker and H. C. Berg, pp. 389–449, Geol. Soc. of Am., Boulder, Colo.

Reiners, P. W., and M. T. Brandon (2006), Using thermochronology to understand orogenic erosion, *Annu. Rev. Earth Planet. Sci.*, *34*, 419–466, doi:10.1146/annurev.earth.34.031405.125202.

Reiners, P. W., et al. (2002), He diffusion and (U-Th)He thermochronometry of zircon: Initial results from Fish Canyon Tuff and Gold Butte, Tectonophysics, *349*, 297–308, doi:10.1016/S0040-1951(02)00058-6.

Sauber, J., et al. (1997), Relation of ongoing deformation rates to the subduction zone processes in southern Alaska, *Geophys. Res. Lett.*, *24*, 2853–2856, doi:10.1029/97GL52979.

Sheaf, M. A., et al. (2003), Exhumation rates in the St. Elias Mountains, Alaska, *Tectonophysics*, *367*, 1–11, doi:10.1016/S0040-1951(03)00124-0.

Sisson, V. B., et al. (1989), Petrologic and age constraints on the origin of a low-pressure/high-temperature metamorphic complex, southern Alaska, *J. Geophys. Res.*, *94*, 4392–4410, doi:10.1029/JB094iB04p04392.

Sisson, V. B., et al. (2003), Geochemical and geochronologic constraints for genesis of a tonalite-trondjemite suite and associated mafic intrusive rocks in the eastern Chugach Mountains, Alaska: A record of ridge-transform subduction, in *Geology of a Transpressional Orogen Developed During Ridge-Trench Interaction Along the North Pacific Margin*, edited by V. B. Sisson et al., pp. 293–326, Geol. Soc. of Am., Boulder, Colo.

Spotila, J., and A. Meigs (2004), Testing glacial limits to mountain building: The buzz saw in the Chugach/St. Elias Range, Alaska, *Eos Trans. AGU*, *85*, Fall Meet. Suppl., Abstract T33D-03.

Spotila, J. A., et al. (2004), Long-term glacial erosion of active mountain belts: The Chugach/St. Elias Range, Alaska, *Geology*, *32*, 501–505, doi:10.1130/G20343.1.

Stüwe, K., et al. (1994), The influence of eroding topography on steady-state isotherms: Application to fission track analysis, *Earth Planet. Sci. Lett.*, *124*, 63–74, doi:10.1016/0012-821X(94)00068-9.

Wahrhaftig, C., et al. (1994), Coal in Alaska, in *The Geology of Alaska*, edited by G. Plafker and H. C. Berg, pp. 937–978, Geol. Soc. of Am., Boulder, Colo.

Whipple, K. X., and B. J. Meade (2006), Orogen response to changes in climatic and tectonic forcing, *Earth Planet. Sci. Lett.*, *243*, 218–228, doi:10.1016/j.epsl.2005.12.022.

Willett, S. (1999), Orogeny and orography: The effects of erosion on the structure of mountain belts, *J. Geophys. Res.*, *104*, 28,957–28,981.

Willett, S. D., and M. T. Brandon (2002), On steady-state in mountain belts, *Geology*, *30*, 175–178, doi:10.1130/0091-7613(2002)030<0175:OSSIMB>2.0.CO;2.

Willett, S., et al. (1993), Mechanical models for the tectonics of doubly vergent compressional orogens, *Geology*, *21*, 371–374, doi:10.1130/0091-7613(1993)021<0371:MMFTTO>2.3.CO;2.

Willett, S. D., et al. (2003), Erosion rates and orogenic-wedge kinematics in Taiwan inferred from fission-track thermochronometry, *Geology*, *31*, 945–948, doi:10.1130/G19702.1.

Wolf, R. A., et al. (1996), Helium diffusion and low temperature thermochronometry of apatite, *Geochim. Cosmochim. Acta*, *60*, 4231–4240, doi:10.1016/S0016-7037(96)00192-5.

Woodward, N. B., et al. (1989), *Balanced Geological Cross-Sections: An Essential Technique in Geologi-*

cal Research and Exploration, Short Course Geol., vol. 6, edited by N. B. Woodward, S. E. Boyer, and J. Suppe, 132 pp., AGU, Washington, D. C.

Zeitler, P. K., et al. (2001), Erosion, Himalayan geodynamics, and the geology of metamorphism, GSA Today, *11*, 4–9, doi:10.1130/1052-5173(2001)011<0004:EHGATG>2.0.CO;2.

Zellers, S. D. (1993), Controls on glacial-marine accumulation rates in the Yakataga Formation, Gulf of Alaska, paper presented at 14th Annual Research Conference on Rates of Geological Processes, Gulf Coast Sect. of Soc. for Sed. Geol., Tulsa, Okla.

Zellers, S. D. (1995), Foraminiferal sequence biostratigraphy and seismic stratigraphy of a tectonically active margin: The Yakataga Formation, northeastern Gulf of Alaska, *Mar. Micropaleontol.*, *26*, 255–271, doi:10.1016/0377-8398(95)00031-3.

Zhang, P., et al. (2001), Increased sedimentation rates and grain sizes 2–4 Myr ago due to the influence of climate change on erosion rates, *Nature*, *410*, 891–897.

J. Garver, Department of Geology, Union College, Schenectady, NY 12308, USA.

S. Johnston, Department of Geosciences, Princeton University, Princeton, NJ 08544, USA.

A. Meigs, Department of Geosciences, Oregon State University, 104 Wilkinson Hall, Corvallis, OR 97330, USA. (meigsa@geo.oregonstate.edu)

J. Spotila, Department of Geology, Virginia Polytechnic Institute and State University, Blacksburg, VA 24061, USA.